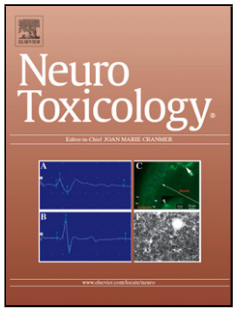

Title: Magnolol protects against trimethyltin-induced neuronal damage and glial activation *in vitro* and *in vivo*

Author: Da Jung Kim Yong Sik Kim

PII: S0161-813X(16)30001-8
DOI: http://dx.doi.org/doi:10.1016/j.neuro.2016.01.001
Reference: NEUTOX 1926

To appear in: *NEUTOX*

Received date: 26-8-2015
Revised date: 5-12-2015
Accepted date: 1-1-2016

Please cite this article as: Kim Da Jung, Kim Yong Sik.Magnolol protects against trimethyltin-induced neuronal damage and glial activation in vitro and in vivo.*Neurotoxicology* http://dx.doi.org/10.1016/j.neuro.2016.01.001

Magnolol protects against trimethyltin-induced neuronal damage and glial activation *in vitro* and *in vivo*

Da Jung KIM[1,2] and Yong Sik KIM[1*]

Department of Pharmacology, Seoul National University College of Medicine, 103 Daehakno, Jongno-gu, Seoul 110-799, Republic of Korea

[1] Department of Pharmacology, Seoul National University College of Medicine, Seoul, Korea

[*]Corresponding author: YS Kim, Department of Pharmacology, Seoul National University College of Medicine, 103 Daehakno, Jongno-Gu, Seoul 110-799, Republic of Korea.
Tel: +82 2 740 8287; Fax: +82 2 745 7996

[2] Present address of Da Jung KIM : Department of Biochemistry and Biomedical Sciences, Seoul National University College of Medicine, 103 Daehakno, Jongno-gu, Seoul 110-799, Republic of Korea.

Details of authors

Yong Sik (given name) KIM(family name)[1*]

Da Jung (given name) KIM (family name)[1,2]

E-mail addresses: kimysu@snu.ac.kr (Yong Sik KIM), dkim3193@hotmail.com (Da Jung KIM)

Highlights

1. TMT induces neuronal cell death and glial activation *in vivo*/*in vitro*
2. Oxidative stress and activation of JNK and p38 MAPKs are involved in TMT toxicity
3. Magnolol suppresses TMT-mediated ROS generation and MAPK activation.

Abstract

Trimethyltin (TMT), an organotin with potent neurotoxic effects by selectively damaging to hippocampus, is used as a tool for creating an experimental model of neurodegeneration. In the present study, we investigated the protective effects of magnolol, a natural biphenolic compound, on TMT-induced neurodegeneration and glial activation *in vitro* and *in vivo*. In HT22 murine neuroblastoma cells, TMT induced necrotic/apoptotic cell death and oxidative stress, including intracellular reactive oxygen species (ROS), protein carbonylation, induction of heme oxygenase-1 (HO-1), and activation of all mitogen-activated protein kinases (MAPKs) family proteins. However, magnolol treatment significantly suppressed neuronal cell death by inhibiting TMT-mediated ROS generation and activation of JNK and p38 MAPKs. In BV-2 microglial cells, magnolol efficiently attenuated TMT-induced microglial activation via suppression of ROS generation and activation of JNK, p38 MAPKs, and nuclear factor-κB (NF-κB) signaling. In an *in vivo* mouse study, TMT induced massive neuronal damage and enhanced oxidative stress at day 2. We also observed a concomitant increase in glial cells and inducible nitric oxide synthase (iNOS) expression on the same day. These features of TMT toxicity were reversed by treatment of magnolol. We observed that p-JNK and p-p38 MAPK levels were increased in the mouse hippocampus at day 1 after TMT treatment and that magnolol blocked TMT-induced JNK and p38 MAPK activation. Magnolol administration prevented TMT-induced hippocampal neurodegeneration and glial activation, possibly through the regulation of TMT-mediated ROS generation and MAPK activation.

Keywords trimethyltin, magnolol, neuronal death, glial activation, oxidative stress, mitogen-activated protein kinases

Abbreviations trimethyltin (TMT); reactive oxygen species (ROS); heme oxygenase (HO)-1; mitogen-activated protein kinases (MAPKs); nuclear factor-κB (NF-κB); inducible nitric oxide synthase (iNOS)

1. Introduction

The systemic administration of trimethyltin (TMT) to humans and rodents induces substantial neuronal cell death, predominantly in the hippocampal neurons in the central nervous system (CNS) resulting in clinical symptoms; cognitive impairment, hyperactivity, aggressiveness, and seizure-like behaviors (Geloso et al, 2011). Although the precise mechanisms by which TMT targets hippocampal neurons have not been established, previous research documented possible risk factors for neuronal cell death, such as excitotoxicity (Gunasekar et al, 2001), intracellular calcium overload and mitochondrial damage (Noraberg et al, 1998). Among these potential mechanisms, the majority of research has focused on oxidative stress (Shin et al, 2005) and neuroinflammation (McPherson et al, 2011) as major pathogenic factors.

Oxidative stress is the result of an imbalance between the production of free radicals, such as reactive oxygen species (ROS) and reactive nitrogen species (RNS), and antioxidant activity (Gandhi et al, 2012). This imbalance is a common risk factor for a range of neurodegenerative diseases since neurons are highly vulnerable to oxidative stress, but free radicals can also target a wide variety of cell types in CNS via disruption of signaling processes and cell homeostasis (Gandhi et al, 2012). The by-products of oxygen consumption can further contribute to the initiation of neuroinflammation (Harry and Kraft, 2008), which has emerged as a key component of various neuropathologies. This condition occurs as a localized response induced primarily by activated microglia (Corvino et al, 2013). Microglia can be activated by external stimuli such as neuronal damage (Lull and Block, 2010) and lipopolysaccharide (LPS) (Harry and Kraft, 2008) and a large amount of oxidative stress can also induce glial activation (Hsieh and Yang, 2013 and Lull and Block, 2010). The activated cells can then secrete a variety of bioactive factors, including cytokines and free radicals, which stimulate a more intensive inflammatory response and neuronal cell death (Corvino et al, 2013, Harry and Kraft, 2008 and Lull and Block, 2010).

Experimental observations supporting the role of oxidative stress and neuroinflammation in TMT-induced neurodegeneration have been reported. For example, ROS formation leading to the dysregulation of glutathione homeostasis (Shin et al, 2005) and increased 4-hydroxynonenal (4-HNE) formation (Huong et al, 2011) provided the prominent evidence of oxidative stress-induced neuron death following TMT exposure. However, a neuroprotective effect was found with the administration of ascorbic acid (Shin et al, 2005) or quercetin (Choi et al, 2012), which were each able to counteract TMT-induced oxidative stress. Evidence of

the neuroinflammatory process during TMT-induced neuronal cell death has also been reported. In TMT experimental models, extensive glial activation occurs concomitantly with hippocampal neuron death (Kim et al, 2014). Typically, microglial activation is regarded as a primary source of inflammatory regulators, such as inducible nitric oxide synthase (iNOS) and cyclooxygenase 2 (COX-2), cytokines such as interleukin (IL)-1α, IL-1β, and tumor necrosis factor α (TNF-α), that might contribute to neuronal death (Corvino et al, 2013, Geloso et al, 2011, Kim et al, 2014 and Lull and Block, 2010). Although it is accepted that the activation of microglia in acute TMT toxicity may be associated with neuronal repair (McPherson et al., 2011), previous studies suggested that suppression of the inflammatory process using neutralizing antibodies against TNF-α (Harry et al, 2002) and indomethacin (Huong et al, 2011) significantly protected neuron cell death in TMT-treated animal models. From these backgrounds, it seems mandatory to find a multi-potent agent possessing antioxidant and anti-inflammatory properties for the protection of TMT-induced neurotoxicity.

Magnolol, which is extracted from *Magnolia officinalis*, is a natural, biphenolic compound. The properties of magnolol have been broadly investigated and include anti-oxidant (Chuang et al, 2013 and Muroyama et al, 2012), anti-inflammatory (Lee et al, 2005), and anti-tumorigenic activities (Seo et al, 2011). Recently, magnolol was suggested to have beneficial effects in the CNS with several studies reporting that magnolol prevented dopaminergic neuronal loss and glial activation in the Parkinson's disease models involving 1-methyl-4-phenyl-1,2,3,6-tetrahydropyridine (Chuang et al, 2013 and Muroyama et al, 2012) or 6-hydroxydopamine (Chen et al, 2011). Moreover, neuronal excitotoxicity and inflammatory responses in microglial cells were also improved by magnolol administration (Chuang et al, 2013). The actual molecular mechanisms or signaling cascades through which magnolol induces CNS protection have not yet been fully clarified; however, some evidence suggest the involvement in a ROS scavenging effect and the regulation of signaling pathways, such as MAPKs and NF-κB signaling, also may be involved (Chen et al, 2014, Chuang et al, 2013 and Lee et al, 2005).

In the present study, therapeutic strategies for using magnolol in TMT-induced neuronal cell death and glial activation were evaluated both *in vivo* and *in vitro*. In cell culture experiments, HT22 neuroblastoma cells and BV-2 microglial cells, which both originated from mice, were used to investigate the protective effects of magnolol on TMT-induced neuronal cell death and microglial activation. Further, beneficial effects of magnolol were

demonstrated in TMT-injected mouse. This neurodegenerative model was also used to provide the roles and mechanisms of MAPK signaling pathways in this response.

2. Materials and methods

2.1 Reagents

Dulbecco's modified Eagle's medium (DMEM), phosphate-buffered saline (PBS), Hank's balanced salt solution (HBSS), fetal bovine serum (FBS), and antibiotic-antimycotic solution were purchased from Gibco (Grand Island, NY, USA). TMT, 2,7-dichlorofluorescein diacetate (DCFH-DA), dimethyl sulfoxide (DMSO), bovine serum albumin, sodium orthovanadate, sodium fluoride, heparin, Tween-20, Hoechst 33258, SB203580, and SP600125 were purchased from Sigma-Aldrich (St. Louis, MO, USA). U0126 was purchased from Calbiochem (San Diego, CA). Rabbit antibodies against p-JNK, p-p38, p-ERK, p38, p-IκBα, IκBα, bcl-2, bax, cleaved caspase-3, ionized calcium binding adaptor molecule 1 (Iba1), and glial fibrillary acidic protein (GFAP) were purchased from Cell Signaling Technologies, Inc. (Beverly, MA, USA). Rabbit anti-JNK, ERK, and NF-κB p65, and mouse anti-NeuN antibodies were purchased from Santa Cruz Biotechnology (Santa Cruz, CA, USA). Mouse anti-iNOS was purchased from BD Biosciences (Franklin Lakes, NJ, USA). Mouse anti-actin was purchased from EMD Millipore (Billerica, MA, USA). The goat anti-mouse and anti-rabbit IgG (HRP-conjugated) secondary antibodies and heme oxygenase 1 (HO-1) primary antibody were from Enzo Life Science (Farmingdale, NY, USA). All other chemicals were purchased from Sigma-Aldrich.

2.2. Cell culture and treatment

Cells were grown at 36°C in a 5% CO_2 incubator in high glucose DMEM supplemented with 10% (v/v) heat-inactivated FBS, 1x antibiotic-antimycotic solution (consisting of 100 units/ml penicillin, 100 μg/ml streptomycin, and 0.25 μg/ml amphotericin B), 2 mM L-glutamine, and 1 mM pyruvate at pH 7.4. At 80% confluence, cells were harvested for subculture. Freshly seeded cells on a culture plate were incubated overnight in a culture medium containing 10% heat-inactivated FBS and antibiotic-antimycotic solution, and then the culture medium was replaced with low-glucose DMEM with 1% FBS for 6 h (for HT22 cells) or 4 h (for BV-2 cells) prior to experimental treatment. Pretreatments of magnolol, vehicle (0.1% DMSO), and each inhibitor, including SB203580 (p38 MAPK inhibitor), SP600125 (JNK MAPK inhibitor), and U0126 (MEK inhibitor), were made 1 h before the

treatment of TMT and dissolved in sterile 0.9% saline. For ROS generation and Western blot, culture medium was changed to low glucose DMEM without FBS and antibiotic-antimycotic solution.

2.3. Cell death determination

To quantify the percentage of cell death, propidium iodide (PI) fluorescence was measured using a microplate reader (Nieminen et al, 1992) with some modifications. In a 96-well tissue culture plate, 1.2×10^3 HT22 cells were seeded per well. Cells were pretreated with magnolol and inhibitors for 1 h before TMT administration and incubated for an additional 24 h. PI (final concentration, 20 μg/ml) was added to the treated wells at 36°C in 5% CO_2 for 30 min. The initial fluorescence from the dead cells was measured by a microplate reader with an excitation at 530 nm and an emission at 630 nm. Next, 2% sodium dodecyl sulfate was added to each well to permeabilize all cells and bind all nuclei with PI. Then, PI fluorescence was re-measured to assess the value of total cells. The percentage of cell death for each sample was calculated as (fluorescence of treated cells/fluorescence of lysed cells) × 100. To measure the number of apoptotic cells, treated cells plated on a 96-well culture plate were incubated with Hoechst 33258 (1 μg/ml) dissolved in PBS for 20 min and then examined using a fluorescence microscope. For each sample, three random fields were captured and examined. The percentage of apoptotic cells were calculated as (number of nuclei with apoptotic morphology/total number of nuclei) × 100.

2.4. Measurement of ROS

Intracellular ROS generation was measured using DCFH-DA assays (Kim and Kim, 2015). In 60 mm^2 tissue culture dishes (BD, Franklin Lakes**,** NJ**,** USA), treated cells at a density of 1×10^6 cells/ml were washed twice with pre-warmed HBSS. Next, the cells were incubated with 15 μM DCFH-DA at 36°C in a CO_2 incubator for 30 min. The cells were again washed twice. A Canto Flow Cytometer (BD Biosciences, CA, USA) was used to quantify the fluorescent cells using excitation at 488 nm and emission at 510 nm. For statistical comparisons, the control value was set at 100%.

2.5. Western blot analysis

Tissue samples or treated cells were lysed with radioimmunoprecipitation assay buffer

(Elpis Biotech, Daejeon, Korea) supplemented with protease and phosphatase inhibitor cocktails (Roche Diagnostics, Rotkreuz, Switzerland) and then separated by centrifugation at 14,000 × g for 20 min at 4°C. The supernatant was collected, and Bradford assays were used to measure the protein concentrations. Equal protein amounts (20 μg) were separated by 10% sodium dodecyl sulfate polyacrylamide gel electrophoresis and then transferred onto a 0.45 μm pore size nitrocellulose membrane (Bio-Rad Laboratories, Hercules, CA, USA) for 1 h at 100 V. After 1 h of blocking in 5% skim milk dissolved in Tris-buffered saline (TBST), pH 7.4, containing 1% Tween-20 for 1 h at room temperature, the membranes were incubated overnight at 4°C with primary antibodies against p-p38 (1:1000), p-JNK (1:1000), p-ERK (1:2000), p-IκBα (1:2000), IκBα (1:2000), p38 (1:2000), JNK (1:2000), ERK (1:2000), iNOS (1:1000), GFAP (1:3000), Iba1(1:2000), HO-1 (1:2000), NeuN (1:2000), cleaved caspase-3 (1:1000), bcl-2 (1:1000), bax (1:1000), or actin (1:2000). After washing with TBST three times for 10 min each, each membrane was incubated with goat anti-rabbit IgG-horseradish peroxidase (HRP) or anti-mouse IgG-HRP for 1 h, and then again rinsed three times with TBST. The blots were immunolabeled with enhanced chemiluminescence HRP substrate (Thermo Fisher Scientific Inc, Rockford, IL, USA) and ChemiDoc^{TM}XRS plus (Bio-Rad laboratories, Hercules, CA, USA) was used to analyze the immunoblot. Actin was used as a total protein loading control.

2.6. Protein carbonylation

To quantify the amount of protein carbonylation, experiments were performed using the OxyBlot Protein Oxidation Detection Kit (EMD Millipore Corporation, Billerica, MA, USA) in accordance with the manufacturer's instructions. In brief, derivatization of the carbonyl groups in each sample was accomplished with 2,4-dinitrophenylhydrazine (DNPH) and then proteins were separated by electrophoresis. After transferring to a nitrocellulose membrane, DNPH expression was detected using an antibody specific to DNPH (1:200).

2.7. Measurement of NO and TNF-α release into the culture medium

BV-2 cells (2.5×10^4) seeded in a 24-well tissue culture plate (Thermo Fisher Scientific Inc.) were treated with TMT in low-glucose DMEM containing 1% (v/v) FBS for 24 h. Then, the medium was removed and separated by centrifugation at 500 × g for 5 min at 4°C. The supernatant fraction was collected for the measurement of NO and TNF-α. For the NO measurements, a general protocol was followed as described previously (Jenkins and Barone,

2004). Briefly, 90 μL of each sample and 10 μL of Griess reagent (containing 0.1% N-[1-naphthyl] ethylenediamine dihydrochloride in 5% H_3PO_4 with 1% sulfanilic acid) was placed in a 96-well tissue culture plate (BD Biosciences**)**. For the standard values, different concentrations of sodium nitrite solution and Griess reagent were placed into the plate. The plate was then gently shaken for 30 min. Absorbance was read on a microplate reader set at 540 nm. The nitrite concentration of each sample was calculated from the standard curve. A TNF-α enzyme-linked immunosorbent assay (ELISA) kit (Abcam, Cambridge, UK) was used to measure the amount of released TNF-α. Each dilution of the standard and each sample were added to the plate, and subsequent experiments were performed according to the manufacturer's protocol. The TNF-α measurements were collected using a microplate reader set at 450 nm. The concentration of each sample was calculated from the standard curve.

2.8. Animals

Five-week-old male ICR mice were obtained from Samtako (Osan, Korea). Mice were maintained for seven days individually in a cage with a 12-hour light/dark cycle and free to access water and food. Procedures for animal care and handling were performed in accordance with the NIH guide for the Care and Use of Laboratory Animals. The Seoul National University Institutional Animal Care and Use Committee (SNU-141208-3) approved the experimental procedures and protocols conducted during this study.

2.9. Drug administration and tissue preparation

Trimethyltin chloride (Sigma-Aldrich, St. Louis, MO, USA) dissolved in sterile 0.9% saline, magnolol (Wako, Osaka, Japan) dissolved in 10% DMSO, 10% cremophore, PBS, and vehicle were provided immediately before administration. After seven days of adaptation, animals were randomly divided into four different groups. Mice received intraperitoneal (i.p.) injections of 25 mg/kg magnolol or vehicle on day 1, 1 h prior to and 2 h after TMT (2.6 mg/kg, i.p.) or 0.9% saline administration. Animals were scarified 1 or 2 days after TMT administration. Mice belonging to the day 1 group were sacrificed 2 h after the final injection of magnolol to maximize its effect. All efforts were made to minimize animal suffering and the number of mice used in the *in vivo* experiments. For histochemical analysis, animals were anesthetized with Avertin (250 mg/kg, i.p.) and perfused via the heart with freshly made PBS containing 2 mM orthovanadate, 20 mM sodium fluoride, 12 units/ml heparin, and a 4%

paraformaldehyde solution, pH 7.4. The mouse brains were removed and stored in 30% sucrose dissolved in PBS following overnight post-fixation in a 4% paraformaldehyde solution. Coronal 30 μm-thick brain sections were used for the appropriate experiments.

2.10. Hippocampal neuronal damage

Fluoro-Jade B (FJB; Millipore, Billerica, MA, USA), possessing a high preference for degenerating neurons, was used to determine the extent of cell death induced by TMT in the hippocampus. Briefly, brain sections were mounted on gelatin-coated glass slides and immersed in a 0.06% potassium permanganate and 0.0004% FJB solution. After washing three times, the sections were dried in the dark. Stained sections were examined using a fluorescence microscope (Axioskop 40; Carl Zeiss, Jena, Germany). The counting of FJB-positive cells in the hippocampus was performed as previously described (Kim et al, 2014). The fraction of cells stained with FJB was calculated as the mean optical density using ImageJ software (NIH, Bethesda, MD, USA). Obtained images were converted into 8-bit grayscale, the colors were inverted, and the threshold value of the image was adjusted until none of the FJB negative cells were detectable. The same threshold was then applied to all images. For each mouse, sections of the hippocampus taken every 180 μm were examined for counting. The total number of FJB positive cells was divided into the number of tissues examined in order to obtain the average intensity.

2.11. Tissue sampling for biochemical assays and Western blots

After 1 and 2 days of TMT administration, animals were decapitated and the hippocampus was isolated. Briefly, a sagittal incision was made to separate the two hemispheres and the cortex, and meningeal tissue surrounding the hippocampus were removed using forceps. The resulting tissue samples were immediately immersed in cold lysis buffer (Elpis Biotech, Daejeon, Korea) containing protease and phosphatase inhibitor cocktails and the samples were sonicated for 10 cycles of 2 sec pulses with 30% amplitude on ice. The protein carbonylation and Western blot analysis procedures were performed as described above.

2.12. Statistical analyses

The data are presented as the mean ± SEM. GraphPad Prism software version 5.0 (San Diego, CA, USA) for Windows was used to analyze the data. One-way analysis of variance

test with Tukey's multiple comparisons was used to examine the differences between groups. A *p* value below 0.05 was considered to be statistically significant.

3. Results

3.1. Magnolol was protective against TMT-induced HT22 cell death

The cytotoxicity of TMT in HT22 cells was initially examined. The cells were incubated with TMT concentrations from 5 μM to 20 μM for 24 h, and then the PI assay was performed to assess the ratio of cell death (Fig. 1a). TMT cytotoxicity increased in a dose-dependent manner with significant increases observed from 10 μM to 20 μM (10 μM, 20.5 ± 4.6%; 15μM, 35.4 ± 3.9%; and 20μM, 48.9 ± 3.5%). Based on these results, 15 μM TMT was selected for use in subsequent experiments. To evaluate the effect of magnolol on TMT-induced cell death, HT22 cells were treated with magnolol (5 μM) or vehicle (0.1% DMSO) for 1 h prior to TMT treatment. With these conditions, magnolol caused an approximately 65% reduction in TMT-induced cell death (TMT, 38.3 ± 1.8%; TMT + magnolol, 13.5 ± 2.6%; Fig. 1b).

To evaluate the effects of magnolol on TMT-induced HT22 cell apoptosis, cells were treated as described above and at 24 h the numbers of fragmented and intact nuclei were counted following Hoechst 33258 staining. A large number of cells with DNA fragmentation were observed in the TMT treatment group, while magnolol pretreatment was shown to effectively reverse TMT-induced cell death (Fig. 2a). Other parameters related to apoptosis were also examined by Western blot. The results clearly demonstrated a decrease in bcl-2 expression. In contrast, the expression of bax and cleaved caspase-3 was increased following TMT treatment (Fig. 2b). These changes induced by TMT were reversed by magnolol pretreatment (Fig. 2b). Together, these data indicate that apoptotic cell death induced by TMT was efficiently prevented with magnolol pretreatment.

3.2. Magnolol reduced TMT-induced HT22 cell oxidative stress

The induction of oxidative stress by TMT has been previously reported (Huong et al, 2011 and Qing et al, 2013). To test the generation of ROS induced by TMT in HT22 cells and effects of magnolol on this induction, ROS production was measured by a DCFH-DA assay performed at each indicated time point. The results showed significantly elevated DCF fluorescence from 1 h to 9 h after initial TMT exposure (Fig. 3a). However, a gradual

reduction in TMT-mediated ROS generation by magnolol was apparent at 1 h after TMT treatment (Fig. 3b). We further examined alternations in protein carbonylation and HO-1 expression at 24 h after TMT treatment. A large quantity of protein carbonylation was detected by TMT, and magnolol suppressed this elevation (Fig. 4a). Induction of HO-1 has been frequently reported as an adaptive response to oxidative stress (Kamalvand et al, 2003). In this experiment, we observed an increased level of HO-1 induced by TMT (Fig. 4b). Moreover, treatment with magnolol attenuated HO-1 expression (Fig. 4b). These results show that magnolol was effective in reducing these parameters in HT22 cells.

3.3. TMT activated MAPKs, but inhibition of p-p38 prevented TMT-induced HT22 cell death

Activation of MAPKs has been documented to play a crucial role in TMT toxicity (Jenkins and Barone., 2004 and Qing et al, 2013). In the present study, we examined MAPK expression levels after TMT exposure in a time-dependent manner. As shown in Fig. 5a, all MAPK family proteins, including JNK, ERK, and p38, were phosphorylated by TMT. In particular, p-JNK and p-p38 were remarkably enhanced at 1 h and 2 h and declined thereafter. The level of p-ERK was also increased from 1 h to 6 h and was then reduced at 8 h post-treatment. To further evaluate the role of MAPKs on TMT-induced neuronal cell death, the activation of each MAPK family member was suppressed by pretreatment of cells with the inhibitors SP600125 (JNK inhibitor), SB203580 (p38 inhibitor), or U0126 (MEK inhibitor). The PI assay was performed after 24 h of TMT treatment in order to determine the proportion of dead cells. Interestingly, a significant suppression of TMT-induced neuronal cell death was observed by treatment of SB203580 as compared to the other inhibitors (Fig. 5b). This finding emphasizes the importance of p38 MAPK activation in TMT-induced HT22 neuronal cell death.

3.4. Magnolol reduced TMT-induced activation of p38 and JNK MAPKs in HT22 cells

An additional investigation was performed to evaluate the effects of magnolol on TMT-induced MAPK activities. After 1 h of TMT treatment, the magnolol-induced down-regulation of TMT-induced p-JNK and p-p38 MAPK formation was detected (Fig. 6). However, magnolol did not influence TMT-mediated p-ERK expression.

3.5. Magnolol suppressed TMT-induced microglial activation via inhibition of ROS

generation/MAPKs and NF-κB activation in BV-2 microglial cells

We recently reported that TMT induces microglial activation in BV-2 cells (Kim and Kim, 2015). To determine if magnolol influences TMT-induced microglial activation, alternations in these parameters were investigated following magnolol treatment. To avoid cytotoxic effects, BV-2 cells were treated with 3 μM TMT. As shown in Fig. 7, TMT treatment induced significant increases in DCF fluorescence and activation of p-JNK and p-38 MAPK at 6 h; however, these results were inhibited by magnolol pretreatment (Fig. 7a, b, c). Magnolol was also effective at suppressing TMT-induced NF-κB activation through reduced phosphorylation of IκBα and degradation of IκBα at 12 h (Fig. 7d).

3.6. Magnolol suppressed TMT-induced BV-2 microglial cell release of NO and TNF-α

iNOS expression determined by Western blot analysis was significantly increased by TMT treatment, but magnolol inhibited this elevation at 12 h (Fig. 8a). Secretion of the soluble factors NO and TNF-α (Fig. 8b,c) after exposure to TMT for 24 h was also notably decreased by magnolol pretreatment. Therefore, magnolol treatment was effective at preventing TMT-induced BV-2 cell microglial activation via inhibition of ROS generation, activation of MAPKs and NF-κB, and release of NO and TNF-α.

3.7. Magnolol protected against TMT-induced neuronal cell death in mouse hippocampus

Following our *in vitro* observations, magnolol protection against TMT-induced cell death and microglial activation, the effect of magnolol on TMT neurotoxicity was evaluated in an *in vivo* study. To first establish the protective effects of magnolol against TMT-induced hippocampus neuron cell death, hippocampus tissue sections obtained at 2 days after TMT exposure were stained with FJB. As shown in Fig. 9a, the number of degenerating neurons in the dentate gyrus following TMT administration was effectively blocked by treatment with magnolol. Magnolol neuroprotection against TMT toxicity were also confirmed by Western blot analysis of NeuN and cleaved caspase-3 expression (Fig. 9b). TMT induced a massive decrease in NeuN expression and an elevation in cleaved caspase-3 compared to the control animals. These changes were markedly prevented by magnolol pretreatment. These results reveal that magnolol protects against TMT-induced neuronal death in the mouse hippocampus.

3.8. Magnolol reduced TMT-mediated oxidative stress in mouse hippocampus

To evalaute the effects of magnolol on TMT-mediated oxidative stress in mice, protein carbonylation and HO-1 expression at 2 days of TMT administration were exvaluated by Western blot analysis (Fig. 10). Protein carbonylation was prominently elevated by TMT alone (Fig. 10a). HO-1 expression was also increased by TMT (Fig. 10b). However, magnolol treatment diminished TMT-induced oxidative stress in the mouse hippocampus (Fig. 10a, b).

3.9. Magnolol decreased TMT-induced glial activation and iNOS expression in mouse hippocampus

Potential alternations in TMT-induced glial activation were also evaluated. Activation of glial cells is one of the more prominent pathologic features of TMT model systems along with granule cell death (McPherson et al, 2011 and Kim et al, 2014). On day 2 of TMT treatment, glial cell expression was analyzed by Western blot analysis. TMT upregulated and magnolol suppressed the expression of GFAP, an astrocyte marker, and Iba1, a marker of microglia, resulting in TMT upregulation and magnolol suppression of glial activation (Fig. 11a, b). Along with glial activation, iNOS expression was also increased by TMT, and magnolol prevented TMT-induced iNOS expression (Fig. 11c). Therefore, magnolol not only prevented neuronal cell death but was also effective in attenuating TMT-induced glial activation and iNOS expression.

3.10. Magnolol decreased TMT-induced activation of JNK and p38 in the mouse hippocampus

In the present study, TMT treatment activated MAPKs, and p38 activation was found to be crucial for TMT-induced neurotoxicity in HT22 cells and p38 and JNK activation for microglial activation in BV-2 cells (Fig. 5; Fig. 7b, c). Evaluation of the relevance of our *in vitro* data in an *in vivo* model system confirmed the presence of altered MAPK activity in the hippocampus at 1 day post-TMT treatment. p-JNK and p-p38 induction in the TMT treatment group was clearly shown by Western blot analysis, but there was no significant change in p-ERK following TMT treatment (Fig. 12). With magnolol treatment, TMT-induced p-JNK and p-p38 was again inhibited in the mouse hippocampus as was observed in the cell culture model system (Fig. 6; Fig. 7b, c). Thus TMT increased p-JNK and p-p38 in the mouse

hippocampus, and magnolol treatment inhibited the TMT-induced upregulation of this protein phosphorylation.

4. Discussion

The present study investigated the effects of magnolol treatment on TMT toxicity both *in vitro* and *in vivo*. The results indicate that magnolol treatment suppressed TMT-induced HT22 cell necrotic/apoptotic cell death and BV-2 cell microglial activation. Furthermore, magnolol protected against neuronal death coincident with the inhibition of glial activation in the hippocampus of TMT-injected mice. Among the regulatory effects exerted by magnolol, prevention of oxidative stress and MAPK activation showed that these changes are essential to the progression of TMT-induced neurodegeneration.

Excessive ROS formation, caused by imbalanced oxygen consumption, has long been implicated as the major factor causing neuronal damage (Gandhi et al, 2012 and Thannickal and Fanburg, 2000) since they are highly reactive and able to damage DNA, proteins, and lipids (Thannickal and Fanburg, 2000). Accumulating evidence indicates that oxidative stress is not only the by-product of cellular metabolism but also contributes to the activation of cell signaling pathways and transcriptional regulatory factors involved in the cellular functions mediated by NF-κB and MAPK family activation (Gao et al, 2013 and Lull and Block, 2010). ROS generation is regarded as a pathogenic factor during TMT toxicity and ROS formation following TMT exposure caused the death of primary neurons (Gunasekar et al, 2001) and several different neuroblastoma cell lines (Jenkins and Barone, 2004, Qing et al, 2013 and Zhang et al, 2006). It is also reported to trigger depletion of glutathione, lipid peroxidation and protein oxidation (Shin et al, 2015) in the murine hippocampus. Following reports on earlier studies, we first confirmed the occurrence of oxidative stress with TMT in our experimental conditions by examining several biomarkers for oxidative stress. From these studies, generation of intracellular ROS at an early time point and an intensive increase in protein carbonylation at a later time point following TMT treatment were both detected in HT22 cells. Furthermore, increased HO-1 expression was detected in these cells. HO-1, an inducible isoform of HO, is used as a marker of oxidative stress that becomes highly expressed in the presence of free radicals and also induces anti-inflammatory and anti-oxidative activities (Kamalvand et al, 2003) In the hippocampus of TMT-treated mice, protein carbonylation and HO-1 expression were significantly increased,

which was consistent with the results in HT22 cells. This oxidative burden provoked neuronal cell loss as shown by Western blot analysis (NeuN and cleaved caspase-3) and histochemical analysis of FJB. These data confirmed the selective neuronal cell death in the mouse hippocampus induced by TMT as has been previously reported (Harry et al, 2003 and Huong et al, 2011), but also strongly suggested the involvement of oxidative stress in this neuropathology.

Neuroinflammation has a close relationship with oxidative stress in various neuropathologies. It is comprised of glial activation and increased production of cytokines in a response to CNS stimuli. External stimuli or intracellular ROS generation can directly activate microglia, which both mediates the response to inflammatory factors and triggers further inflammatory responses and the generation of free radicals (Corvino et al, 2013 and Harry and Kraft, 2008). In TMT model systems, glial activation along with enhanced production of the pro-inflammatory factors IL-1β, IL-12, TNF-α, NO, and ROS have been reported (Noraberg et al, 1998 and Shin et al, 2005). Microglial activation has been suggested as a dominant feature for inflammatory processes since potentiated neuronal cell death and elevated levels of the cytokines IL-1β, IL-6, and TNF-α were detected from a co-culture of primary neurons with microglia (Eskes et al, 2003), and elevation of pro-inflammatory cytokine mRNA levels belonging to the M1 stage (Kim et al, 2014) were also found under TMT exposure.

Although there is existing evidence that activated microglia contribute to cell proliferation and differentiation (Tambuyzer et al, 2009), it has been predominantly suggested to be deleterious to neuronal survival during TMT toxicity . Typically, enhanced TNF-α production is apparent with microglial activation (Eskes et al, 2003 and Kim et al, 2014) and the severity of neuronal death following TMT intoxication improves with the administration of a neutralizing antibody to TNF-α (Harry et al, 2002), resulting in the proposition that TNF-α has a critical role during TMT-mediated neuronal death. Previously we have shown that in BV-2 microglial cells, TMT directly activates microglia via NADPH oxidase and MAPKs (Kim and Kim, 2015). Therefore, data from the *in vivo* experiments in the present study showed that the TMT-induced activation of glial cells coincided with neuronal cell death in the hippocampus. We also observed a significant increase in iNOS expression by day 2 after TMT administration, and an extensive amount of iNOS in the hippocampus, most typically

focused within the damaged region, was seen upon immunohistochemical examination (data not shown). In general, induction of iNOS is tightly linked with inflammatory processes such that it is activated by pro-inflammatory cytokines or foreign pathogens to increase NO generation for the defense of glial cells (Harry and Kraft, 2008 and Lull and Block, 2010). A by-product of iNOS activation, NO is then able to mediate either excessive oxidative stress and damage or additional inflammatory responses (Harry and Kraft, 2008, Latini et al, 2010 and Lull and Block, 2010). A recent study (Yang et al, 2012) reported the elevation of pro-inflammatory mediators COX-2 and iNOS in the hippocampus of the TMT-injured brain 4 days after TMT exposure. This result is in agreement with the present data; however, other reports contradicted our results and showed no alteration in iNOS mRNA in the mouse hippocampus until after 3 days of TMT exposure (Bruccoleri et al, 2000).

A number of researchers have been working to discover new drug candidates for use with the neurodegenerative diseases associated with limbic system dysfunction. With TMT-mediated neuronal damage, repeated administration of ascorbic acid to rats for 3 weeks partially protected against TMT-induced neuronal damage and cognitive impairment (Shin et al, 2005). A pyridoindole antioxidant also prevented TMT-induced rat pyramidal cell death in CA1 area (Gasparova et al, 2014). Flavonoid dietary supplements such as *Ginkgo biloba* extract (Kaur et al, 2013), quercetin (Choi et al, 2012), and rutin (Koda et al, 2009) have also been investigated as potential measures to counteract the neuronal damage induced by TMT. Rutin supplementation (Koda et al, 2009) was also reported to suppress microglia activation and cytokine production in TMT-treated rats. One anti-inflammatory strategy was the administration of TNF-α neutralizing antibodies, which provided remarkable neuroprotection in mice (Harry et al, 2002). In addition, indomethacin, a COX-2 inhibitor, provided partial neuroprotection in TMT-treated mice (Huong et al, 2011). Even though these pharmacological agents are reported to display potential therapeutic benefits such as scavenging free radicals or suppressing glial activation, a variety of different pathogenic mechanisms can occur simultaneously during neurodegeneration, necessitating the use of a multi-functional therapeutic agent to provide optimal protection. Thus, the rationale for the investigation of therapies that possess both antioxidant and anti-inflammatory properties was suggested to counter TMT toxicity, and we chose to evaluate magnolol as a tool for improving the neuropathogenic features.

Magnolol is a natural, biphenolic compound that is able to cross the blood-brain barrier (Muroyama et al, 2012). The diverse biological activities of magnolol have been extensively documented and include anti-tumorigenic (Seo et al, 2011) and anti-inflammatory (Chuang et al, 2013 and Lee et al, 2005) activities. In addition, regulation of oxidative stress has been frequently reported *in vivo* (Chen et al, 2014 and Muroyama et al, 2012) and *in vitro* (Chuang et al, 2013). Current research has focused on the benefits of magnolol in treating neuropathogenesis. For instance, magnolol is reported to exert anti-inflammatory effects through the regulation of p38 MAPK, CHOP, and nitrotyrosine production in an ischemic injury model (Chen et al, 2014) and attenuation of dopaminergic cell loss (Chen et al, 2011) and glial activation (Muroyama et al, 2012) by anti-oxidative mechanisms in Parkinson's disease models. Based on current evidence, the effects of magnolol on TMT toxicity were evaluated in the present study. The use of magnolol as a therapeutic antioxidant agent ameliorated TMT-mediated oxidative stress, thereby protecting against neuronal death in the mouse hippocampus and HT22 cell necrotic/apoptotic cell death. Certain anti-inflammatory properties of magnolol were also revealed. In BV-2 cells, magnolol regulated microglial activation and production of inflammatory factors (iNOS, NO, and TNF-α) through the inhibition of NF-κB activation. In mice, activation of astrocytes and microglia following TMT administration was prevented by treatment with magnolol at day 2. Effective suppression of iNOS protein was shown by magnolol on the same day. These results were similar to those from previous investigations that highlighted anti-oxidative and anti-inflammatory mechanisms against external stimuli such as LPS (Chuang et al, 2013 and Zhou et al, 2008), interferon gamma (IFN-γ) (Chuang et al, 2013), and foreign pathogens (Lee et al, 2005).

The activation of MAPKs is one important consequence of oxidative stress. Once the MAPK signaling pathway is initiated, it can regulate multiple cellular functions, such as cell proliferation, differentiation, and death. While inflammatory responses occur in a variety of circumstances, MAPK signaling cascades can be crucial contributors. For example, LPS (Chuang et al, 2013) and rotenone (Gao et al, 2013) activate microglia via p38 activation, and amyloid beta-mediated microglial activation requires JNK and p38 activation (Park et al, 2012). The role of MAPK activation in TMT toxicity has been emphasized, including JNK and ERK in SH-SY5Y cell death (Qing et al, 2013), p38 in PC12 cell death (Jenkins and Barone., 2004) and JNK and p38 in BV-2 cell microglial activation (Kim and Kim., 2015). Despite, most of these reports were conducted using cell culture system. A limited number of

studies have confirmed the role of MAPK modulation using TMT-injured mice; activation of JNK in CA1 pyramidal and dentate gyrus cell layers from 16 h to 24 h after TMT treatment (Ogita et al, 2004), suggesting the possible involvement of JNK activation in TMT-induced neuronal cell death in the brain. Also, blocking JNK with SP600125 partially protected against TMT-mediated neuronal death in mouse primary cortical neurons (Shuto et al, 2009). From this background, our efforts were made to evaluate the role of MAPK signaling pathway in TMT toxicity and its modulation by magnolol as a therapeutic agent *in vitro* and *in vivo*.

In the present study, we found that phosphorylation of all of the MAPK family proteins following activation by TMT treatment, and inhibition of p-p38 by SB203580, a p38 MAPK inhibitor, significantly prevented TMT-induced neuronal HT22 cell death. Again, magnolol treatment reduced p-JNK and p-p38 levels in the same experimental condition. Furthermore, p-JNK and p-p38 were both associated with TMT-induced microglial activation in BV-2 cells, and magnolol achieved a suppressive effect on both microglial activation and the production of inflammatory bioactive factors. Based on these findings, MAPK protein family activation may be essential for TMT-induced neuronal cell death and microglial activation, and magnolol has the capacity to protect against both of these responses. We further demonstrated that TMT can activate any MAPK family member in the hippocampus under our current experimental conditions, and that magnolol is capable of regulating this TMT-induced MAPK activation. As a result, we observed the activation of p38 in addition to JNK activation in the hippocampus at day 1 after TMT administration. The inhibitory effects on p-p38 and p-JNK were also mediated by magnolol when given on the same day of the experiment. These findings from *in vitro* and *in vivo* experiments suggest a correlation between MAPK signaling activation during TMT-induced neurodegeneration and its modulation by magnolol. In particular, our *in vivo* data suggest a possible role for p38 and JNK activation in the TMT-induced neurodegeneration and glial activation in the hippocampus. Additional investigations are needed to define which type of cells in brain is the main source for MAPK activation following TMT treatment and the specific roles for MAPK activation during TMT-induced neuronal damage *in vivo*.

5. Conclusions

In the present study, we demonstrated that oxidative stress and MAPK signaling

components are induced by TMT toxicity. Magnolol regulates TMT-mediated ROS generation and MAPK activation. Taken together, magnolol possesses strong potential as a therapeutic for combating neurodegenerative diseases associated with oxidative burden and neuroinflammation.

Conflict of interest

The authors declare that there is no conflict of interests regarding the publication of this paper.

Acknowledgement

This work was supported by the Education and Research Encouragement Fund of Seoul National University Hospital (2016).

References

[1] Bruccoleri A, Harry GJ. Chemical-induced hippocampal neurodegeneration and elevations in TNFalpha, TNFbeta, IL-1alpha, IP-10, and MCP-1 mRNA in osteopetrotic (op/op) mice. J Neurosci Res. 2000 Oct 1;62(1):146-55.

[2] Chen HH, Lin SC, Chan MH. Protective and restorative effects of magnolol on neurotoxicity in mice with 6-hydroxydopamine-induced hemiparkinsonism. Neurodegener Dis. 2011;8(5):364-74. doi: 10.1159/000323872.

[3] Chen JH, Kuo HC, Lee KF, Tsai TH. Magnolol protects neurons against ischemia injury via the downregulation of p38/MAPK, CHOP and nitrotyrosine. Toxicol Appl Pharmacol. 2014 Sep 15;279(3):294-302. doi: 10.1016/j.taap.2014.07.005.

[4] Choi GN, Kim JH, Kwak JH, Jeong CH, Hee RJ, Lee U, Heo HJ. Effect of quercetin on learning and memory performance in ICR mice under neurotoxic trimethyltin exposure. Food Chemistry. 2012; (132(2012) 1019-1024.

[5] Chuang DY, Chan MH, Zong Y, Sheng W, He Y, Jiang JH, Simonyi A, Gu Z, Fritsche KL, Cui J, Lee JC, Folk WR, Lubahn DB, Sun AY, Sun GY. Magnolia polyphenols attenuate oxidative and inflammatory responses in neurons and microglial cells. J Neuroinflammation. 2013 Jan 29;10:15. doi: 10.1186/1742-2094-10-15.

[6] Corvino V, Marchese E, Michetti F, Geloso MC. Neuroprotective strategies in hippocampal neurodegeneration induced by the neurotoxicant trimethyltin. Neurochem Res. 2013 Feb;38(2):240-53. doi: 10.1007/s11064-012-0932-9.

[7] Eskes C, Juillerat-Jeanneret L, Leuba G, Honegger P, Monnet-Tschudi F. Involvement of microglia-neuron interactions in the tumor necrosis factor-alpha release, microglial activation, and neurodegeneration induced by trimethyltin. J Neurosci Res. 2003 Feb 15;71(4):583-90.

[8] Gandhi S, Abramov AY. Mechanism of oxidative stress in neurodegeneration. Oxid Med Cell Longev. 2012;2012:428010. doi: 10.1155/2012/428010.

[9] Gao F, Chen D, Hu Q, Wang G. Rotenone directly induces BV2 cell activation via the p38 MAPK pathway. PLoS One. 2013 Aug 20;8(8):e72046. doi: 10.1371/journal.pone.0072046.

[10] Gasparova Z, Stara V, Janega P, Navarova J, Sedlackova N, Mach M, Ujhazy E. Pyridoindole antioxidant-induced preservation of rat hippocampal pyramidal cell number linked with reduction of oxidative stress yet without influence on cognitive deterioration in

Alzheimer-like neurodegeneration. Neuro Endocrinol Lett. 2014;35(6):454-62.

[11] Geloso MC, Corvino V, Michetti F. Trimethyltin-induced hippocampal degeneration as a tool to investigate neurodegenerative processes. Neurochem Int. 2011 Jun;58(7):729-38. doi: 10.1016/j.neuint.2011.03.009.

[12] Gunasekar P, Li L, Prabhakaran K, Eybl V, Borowitz JL, Isom GE. Mechanisms of the apoptotic and necrotic actions of trimethyltin in cerebellar granule cells. Toxicol Sci. 2001 Nov;64(1):83-9.

[13] Harry GJ, Bruccoleri A, Lefebvre d'Hellencourt C. Differential modulation of hippocampal chemical-induced injury response by ebselen, pentoxifylline, and TNFalpha-, IL-1alpha-, and IL-6-neutralizing antibodies. J Neurosci Res. 2003 Aug 15;73(4):526-36.

[14] Harry GJ, Kraft AD. Neuroinflammation and microglia: considerations and approaches for neurotoxicity assessment. Expert Opin Drug Metab Toxicol. 2008 Oct;4(10):1265-77. doi: 10.1517/17425255.4.10.1265 .

[15] Harry GJ, Tyler K, d'Hellencourt CL, Tilson HA, Maier WE. Morphological alterations and elevations in tumor necrosis factor-alpha, interleukin (IL)-1alpha, and IL-6 in mixed glia cultures following exposure to trimethyltin: modulation by proinflammatory cytokine recombinant proteins and neutralizing antibodies. Toxicol Appl Pharmacol. 2002 May 1;180(3):205-18.

[16] Hsieh HL, Yang CM. Role of redox signaling in neuroinflammation and neurodegenerative diseases. Biomed Res Int. 2013;2013:484613. doi: 10.1155/2013/484613.

[17] Huong NQ, Nakamura Y, Kuramoto N, Yoneyama M, Nagashima R, Shiba T, Yamaguchi T, Hasebe S, Ogita K. Indomethacin ameliorates trimethyltin-induced neuronal damage in vivo by attenuating oxidative stress in the dentate gyrus of mice. Biol Pharm Bull. 2011;34(12):1856-63.

[18] Jenkins SM, Barone S. The neurotoxicant trimethyltin induces apoptosis via caspase activation, p38 protein kinase, and oxidative stress in PC12 cells. Toxicol Lett. 2004 Feb 28;147(1):63-72.

[19] Kamalvand G, Pinard G, Ali-Khan Z. Heme-oxygenase-1 response, a marker of oxidative stress, in a mouse model of AA amyloidosis. Amyloid. 2003 Sep;10(3):151-9

[20] Kaur S, Chhabra R, Nehru B. Ginkgo biloba extract attenuates hippocampal neuronal loss and cognitive dysfunction resulting from trimethyltin in mice. Phytomedicine. 2013 Jan 15;20(2):178-86. doi: 10.1016/j.phymed.2012.10.003.

[21] Kim DJ and Kim YS. Trimethyltin-Induced Microglial Activation via NADPH Oxidase

and MAPKs Pathway in BV-2 Microglial Cells. Mediators of Inflammation,2015 (2015) Article ID 729509, 14 pages, doi:10.1155/2015/729509

[22] Kim J, Yang M, Son Y, Jang H, Kim D, Kim JC, Kim SH, Kang MJ, Im HI, Shin T, Moon C. Glial activation with concurrent up-regulation of inflammatory mediators in trimethyltin-induced neurotoxicity in mice. Acta Histochem. 2014 Oct;116(8):1490-500. doi: 10.1016/j.acthis.2014.09.003.

[23]Koda T, Kuroda Y, Imai H. Rutin supplementation in the diet has protective effects against toxicant-induced hippocampal injury by suppression of microglial activation and pro-inflammatory cytokines: protective effect of rutin against toxicant-induced hippocampal injury. Cell Mol Neurobiol. 2009 Jun;29(4):523-31. doi: 10.1007/s10571-008-9344-4..

[24] Latini L, Geloso MC, Corvino V, Giannetti S, Florenzano F, Viscomi MT, Michetti F, Molinari M. Trimethyltin intoxication up-regulates nitric oxide synthase in neurons and purinergic ionotropic receptor 2 in astrocytes in the hippocampus. J Neurosci Res. 2010 Feb 15;88(3):500-9. doi: 10.1002/jnr.22238.

[25] Lee J, Jung E, Park J, Jung K, Lee S, Hong S, Park J, Park E, Kim J, Park S, Park D. Anti-inflammatory effects of magnolol and honokiol are mediated through inhibition of the downstream pathway of MEKK-1 in NF-kappaB activation signaling. Planta Med. 2005 Apr;71(4):338-43.

[26] Lull ME, Block ML. Microglial activation and chronic neurodegeneration. Neurotherapeutics. 2010 Oct;7(4):354-65. doi: 10.1016/j.nurt.2010.05.014.

[27] McPherson CA, Kraft AD, Harry GJ. Injury-induced neurogenesis: consideration of resident microglia as supportive of neural progenitor cells. Neurotox Res. 2011 Feb;19(2):341-52. doi: 10.1007/s12640-010-9199-6.

[28] Muroyama A, Fujita A, Lv C, Kobayashi S, Fukuyama Y, Mitsumoto Y. Magnolol Protects against MPTP/MPP(+)-Induced Toxicity via Inhibition of Oxidative Stress in In Vivo and In Vitro Models of Parkinson's Disease. Parkinsons Dis. 2012;2012:985157. doi: 10.1155/2012/985157.

[29] Nieminen AL, Gores GJ, Bond JM, Imberti R, Herman B, Lemasters JJ. A novel cytotoxicity screening assay using a multiwell fluorescence scanner. Toxicol Appl Pharmacol. 1992 Aug;115(2):147-55.

[30] Noraberg J, Gramsbergen JB, Fonnum F, Zimmer J. Trimethyltin (TMT) neurotoxicity in organotypic rat hippocampal slice cultures. Brain Res. 1998 Feb 9;783(2):305-15.

[31] Ogita K, Nitta Y, Watanabe M, Nakatani Y, Nishiyama N, Sugiyama C, Yoneda Y. In vivo

activation of c-Jun N-terminal kinase signaling cascade prior to granule cell death induced by trimethyltin in the dentate gyrus of mice. Neuropharmacology. 2004 Sep;47(4):619-30.

[32] Park SY, Jin ML, Kim YH, Kim Y, Lee SJ. Anti-inflammatory effects of aromatic-turmerone through blocking of NF-κB, JNK, and p38 MAPK signaling pathways in amyloid β-stimulated microglia. Int Immunopharmacol. 2012 Sep;14(1):13-20. doi: 10.1016/j.intimp.2012.06.003.

[33] Qing Y, Liang Y, Du Q, Fan P, Xu H, Xu Y, Shi N. Apoptosis induced by trimethyltin chloride in human neuroblastoma cells SY5Y is regulated by a balance and cross-talk between NF-κB and MAPKs signaling pathways. Arch Toxicol. 2013 Jul;87(7):1273-85. doi: 10.1007/s00204-013-1021-9.

[34] Seo JU, Kim MH, Kim HM, Jeong HJ. Anticancer potential of magnolol for lung cancer treatment. Arch Pharm Res. 2011 Apr;34(4):625-33. doi: 10.1007/s12272-011-0413-8.

[35] Shin EJ, Suh SK, Lim YK, Jhoo WK, Hjelle OP, Ottersen OP, Shin CY, Ko KH, Kim WK, Kim DS, Chun W, Ali S, Kim HC. Ascorbate attenuates trimethyltin-induced oxidative burden and neuronal degeneration in the rat hippocampus by maintaining glutathione homeostasis. Neuroscience. 2005;133(3):715-27.

[36] Shin EJ, Nam Y, Tu TH, Lim YK, Wie MB, Kim DJ, Jeong JH, Kim HC. Protein kinase Cδ mediates trimethyltin-induced neurotoxicity in mice in vivo via inhibition of glutathione defense mechanism. Arch Toxicol. 2015 Apr 18.

[37] Shuto M, Seko K, Kuramoto N, Sugiyama C, Kawada K, Yoneyama M, Nagashima R, Ogita K. Activation of c-Jun N-terminal kinase cascades is involved in part of the neuronal degeneration induced by trimethyltin in cortical neurons of mice. J Pharmacol Sci. 2009 Jan;109(1):60-70.

[38] Tambuyzer BR, Ponsaerts P, Nouwen EJ. Microglia: gatekeepers of central nervous system immunology. J Leukoc Biol. 2009 Mar;85(3):352-70. doi: 10.1189/jlb.0608385.

[39] Thannickal VJ, Fanburg BL. Reactive oxygen species in cell signaling. Am J Physiol Lung Cell Mol Physiol. 2000 Dec;279(6):L1005-28.

[40] Yang M, Kim J, Kim T, Kim SH, Kim JC, Kim J, Takayama C, Hayashi A, Joo HG, Shin T, Moon C. Possible involvement of galectin-3 in microglial activation in the hippocampus with trimethyltin treatment. Neurochem Int. 2012 Dec;61(7):955-62. doi: 10.1016/j.neuint.2012.09.015.

[41] Zhang L, Li L, Prabhakaran K, Borowitz JL, Isom GE. Trimethyltin-induced apoptosis is associated with upregulation of inducible nitric oxide synthase and Bax in a hippocampal cell

line. Toxicol Appl Pharmacol. 2006 Oct 1;216(1):34-43.

[42] Zhou HY, Shin EM, Guo LY, Youn UJ, Bae K, Kang SS, Zou LB, Kim YS. Anti-inflammatory activity of 4-methoxyhonokiol is a function of the inhibition of iNOS and COX-2 expression in RAW 264.7 macrophages via NF-kappaB, JNK and p38 MAPK inactivation. Eur J Pharmacol. 2008 May 31;586(1-3):340-9. doi: 10.1016/j.ejphar.2008.02.044.

Figure and legends

(a) (b)

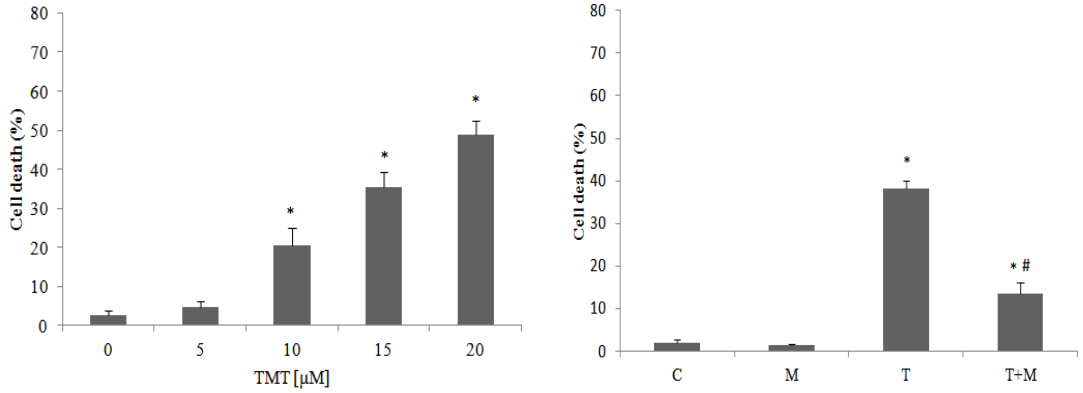

Fig. 1. Magnolol protected against TMT-induced HT22 neuronal cell death. (a) Cells were treated with various concentrations of TMT (5–20 μM) for 24 h. (b) Cells were pretreated with 5 μM magnolol or vehicle (0.1% DMSO) for 1 h and then treated with 15 μM TMT or vehicle (saline) for 24 h, and the PI assay was performed to access the percentage of dead cells. Data are presented as the mean ± SEM (n = 5). *$p < 0.05$ compared with the control value, $^{\#}p < 0.05$ compared with the value following TMT alone. C: control, M: magnolol, T: TMT, T+M: TMT + magnolol

(a) (b)

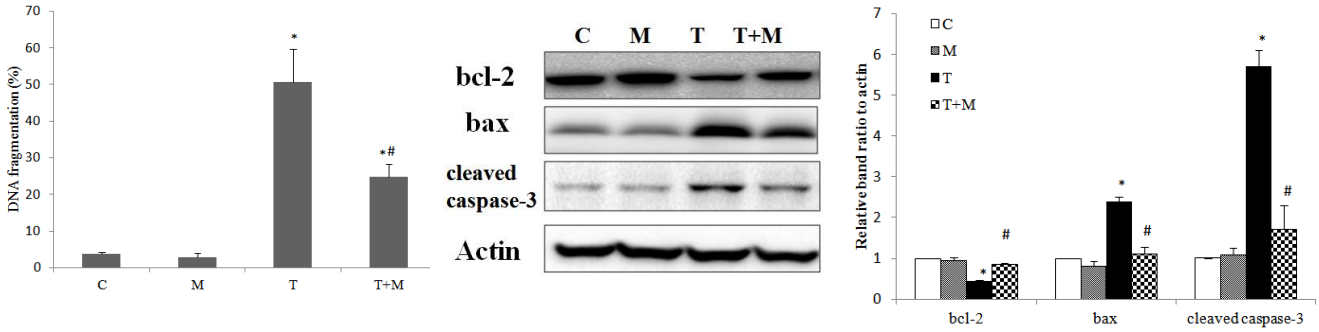

Fig. 2. Magnolol protected against TMT-induced HT22 cell DNA fragmentation and apoptosis. (a) After 24 h of TMT treatment, cells were stained with Hoechst 33258 and images were captured. To assess the ratio of DNA fragmentation, images of three random fields per sample were captured using a fluorescence microscope and a 20× objective, and the number of apoptotic nuclei was compared to the total number of nuclei. (b) After 24 h of TMT treatment, cells were collected and subjected to Western blot analysis. The bar graphs represent the band intensity of bcl-2, bax and cleaved caspase-3 normalized to actin expression. Data are presented as the mean ± SEM (n = 4). $*p < 0.05$ compared with the control value, $^{\#}p < 0.05$ compared with the value following TMT alone. C: control, M: magnolol, T: TMT, T+M: TMT + magnolol

(a) (b)

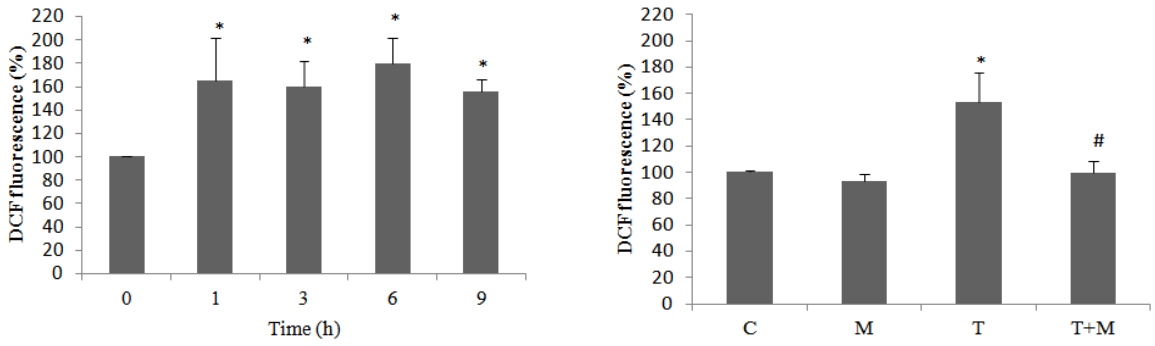

Fig. 3. Magnolol suppressed TMT-induced ROS generation in HT22 cells. (a) TMT-treated cells were incubated for the indicated periods of time (0 –9 h) and stained with DCFH-DA for 30 min. (b) Magnolol or vehicle pretreatment for 1 h prior to TMT. After 1 h of TMT exposure, the DCFH-DA assay was performed. The DCF fluorescence of each sample was analyzed by flow cytometry, with the value obtained at 0 h or control set as 100%. Data are presented as the mean ± SEM (n = 4). *$p < 0.05$ compared with the control value, $^{\#}p < 0.05$ compared with the value following TMT alone. C: control, M: magnolol, T: TMT, T+M: TMT + magnolol

(a) (b)

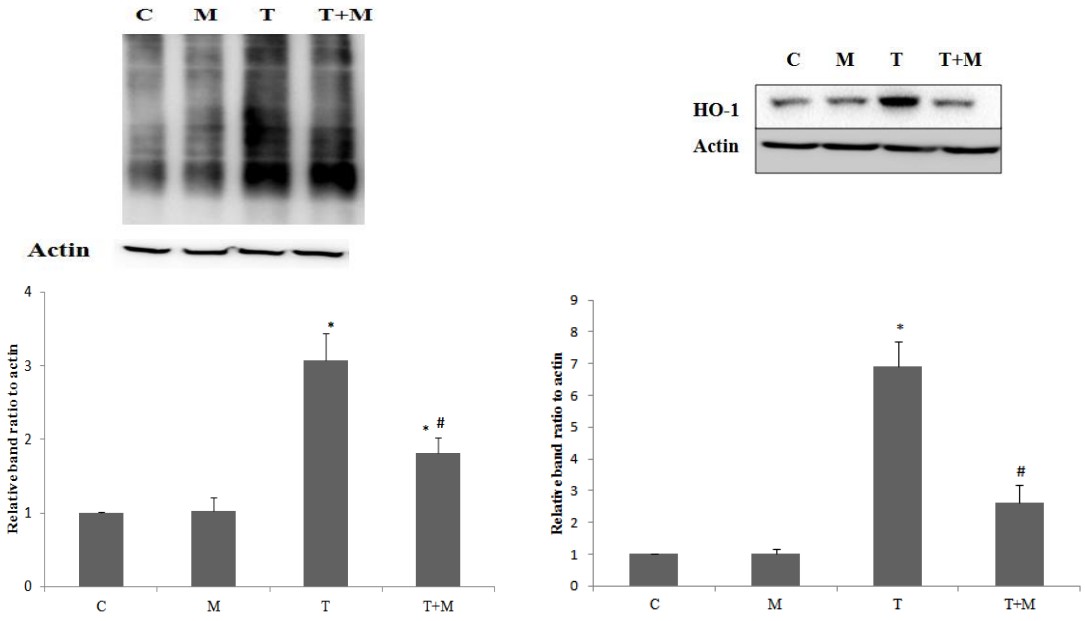

Fig. 4. Magnolol suppressed TMT-induced protein carbonylation and HO-1 expression in HT22 cells. Cells treated with TMT for 24 h were collected and subjected to Western blot analysis of (a) protein carbonylation and (b) HO-1 expression. The bar graphs represent the band intensity of protein carbonyls and HO-1 normalized to actin expression. Data are presented as the mean ± SEM (n = 4). *$p < 0.05$ compared with the control value, $^{\#}p < 0.05$ compared with the value following TMT alone. C: control, M: magnolol, T: TMT, T+M: TMT + magnolol

(a)

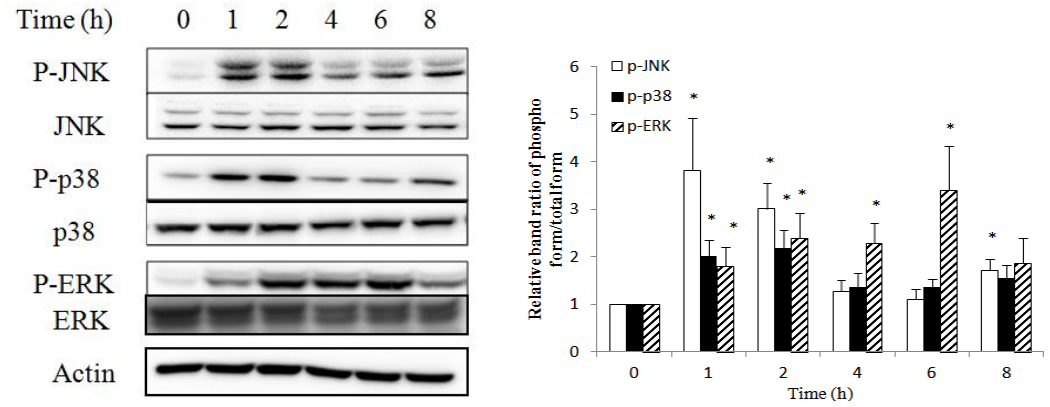

(b)

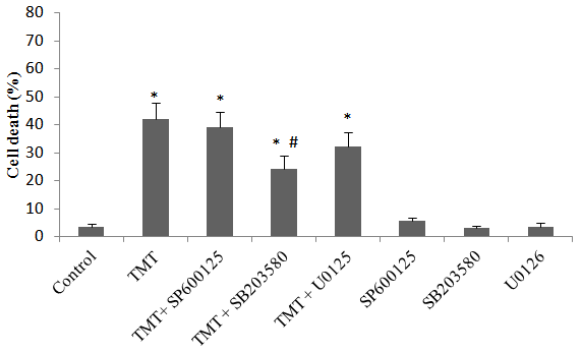

Fig. 5. TMT induced HT22 cell MAPK activation and SB203580 protected against TMT-induced cell death. (a) MAPK activation in TMT-treated cells was analyzed by Western blot at each treatment time period. The bar graphs represent the band intensity of each phosphorylated form of MAPK normalized to total protein. (b) Cells were pretreated with an inhibitor (10 μM SP600125, 10 μM SB203580, or 10 μM U0126) or vehicle (DMSO 0.1%) for 1 h prior to TMT treatment. After 24 h of TMT treatment, the PI assay was performed to measure the amount of dead cells. Data are presented as the mean ± SEM (n = 7). *$p < 0.05$ compared with the control group, $^{\#}p < 0.05$ compared with the value following TMT treatment alone. C: control, T: TMT

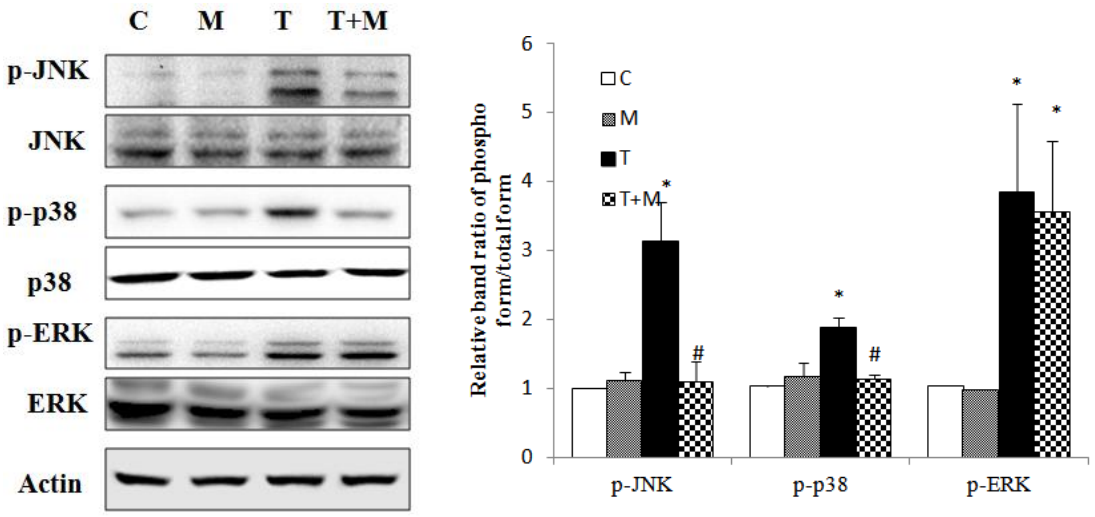

Fig. 6. Magnolol suppressed TMT-induced p-JNK and p-p38 expression in HT22 cells. Treated cells were collected following 1 h of TMT treatment and subjected to Western blot analysis. The bar graph represents the band intensity of p-JNK, p-ERK, and p-p38 protein forms normalized to the total expression of each protein. Data are presented as the mean ± SEM (n = 3–6). *$p < 0.05$ compared with the control group, $^{\#}p < 0.05$ compared with the TMT treatment alone. C: control, M: magnolol, T: TMT, T+M: TMT + magnolol

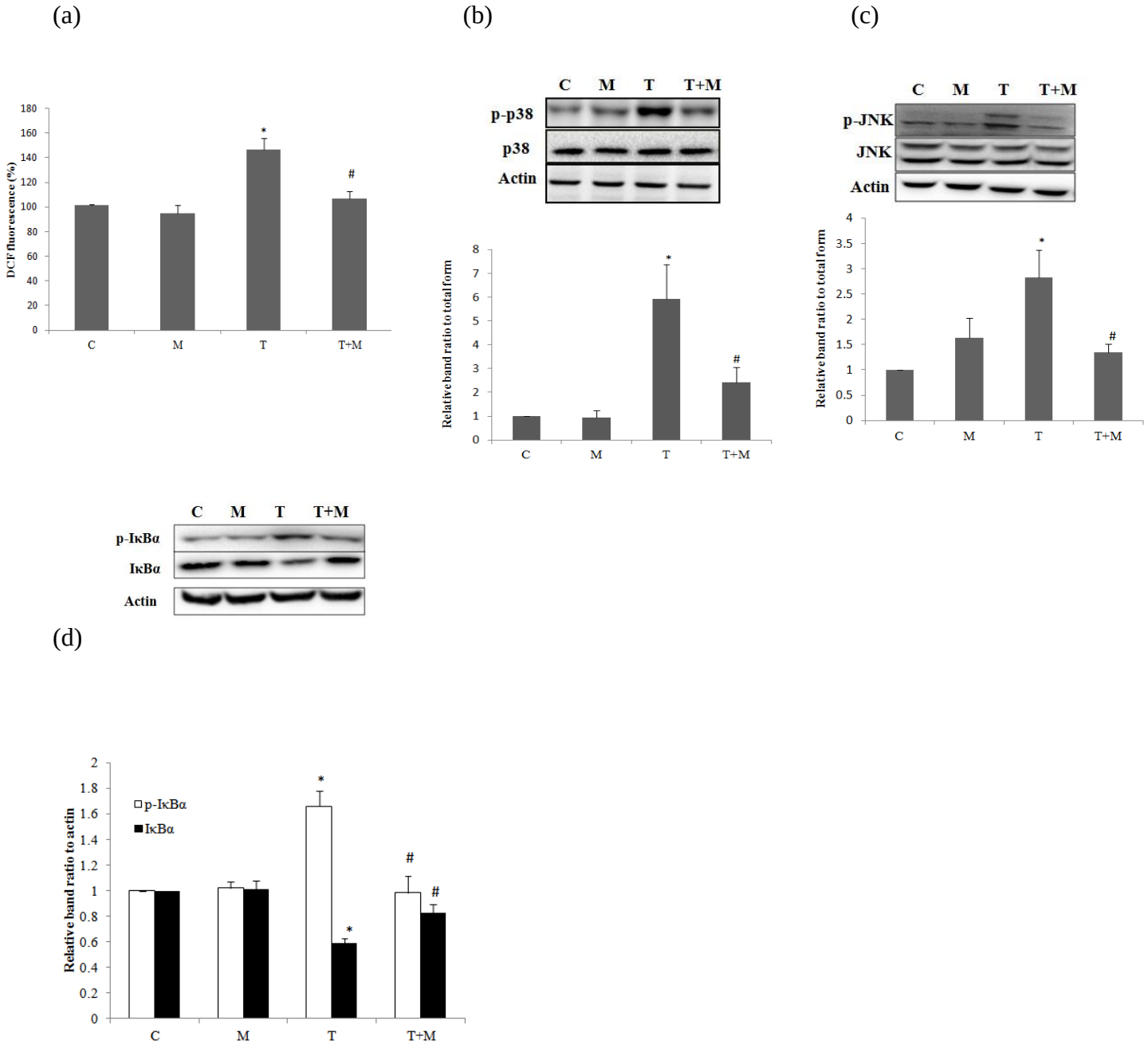

Fig. 7. Magnolol suppressed TMT-induced ROS generation and attenuated MAPK and NF-kB activation in BV-2 microglial cells. Cells were pretreated with magnolol (5 μM) or vehicle (DMSO 0.1%) for 1 h prior to TMT treatment. After 6 h of incubation with TMT, (a) the DCFH-DA assay was performed. The DCF fluorescence of each sample was analyzed by flow cytometry, with the values obtained for the control group set at 100%. For Western blot analysis of (b) p-p38 and (c) p-JNK, cells were treated with TMT for 6 h, and (d) IκBα phosphorylation and IκBα degradation for 12 h. The bar graphs in the Western blot analysis represent the band intensity for p-p38, p-JNK, p-IκBα, and IκBα blots, normalized to the appropriate total amount of protein. Data are presented as the mean ± SEM (n = 4–6). *p < 0.05 compared with the control group, $^{\#}p$ < 0.05 compared with the value following TMT treatment alone. C: control, M: magnolol, T: TMT, T+M: TMT + magnolol

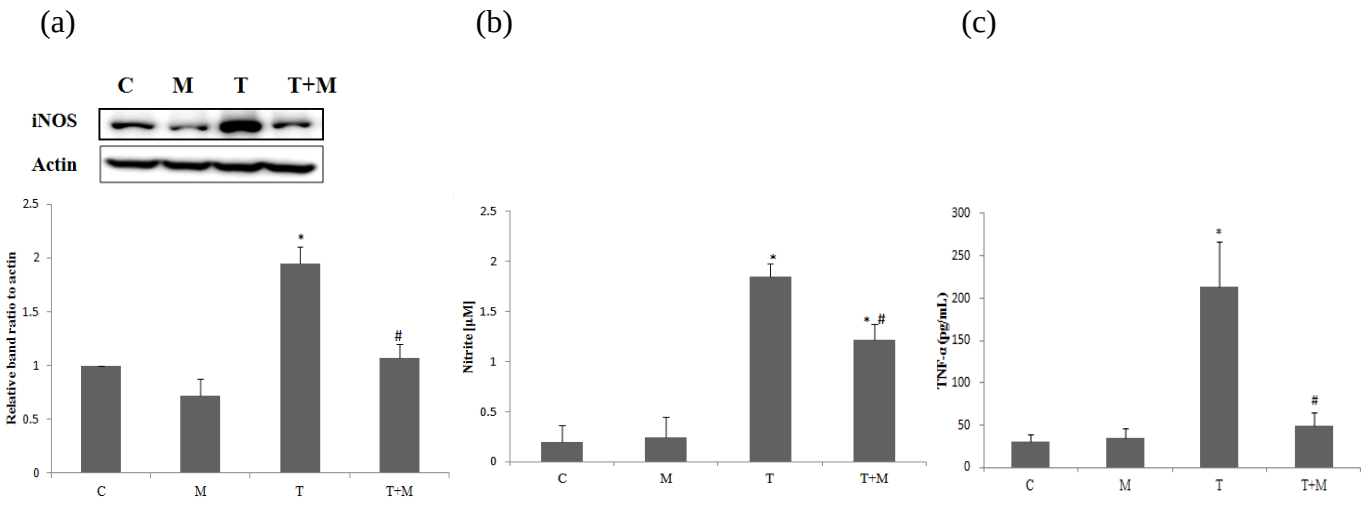

Fig. 8. Magnolol decreased the BV-2 microglial cell expression of iNOS and the release of NO and TNF-α that was induced by TMT. Treated cells were processed for Western blot analysis of (a) iNOS at 12 h. The bar graph in the Western blot analysis represents the band intensity of iNOS normalized to actin. The cell culture media obtained after 24 h of treatment was collected to assess the level of (b) NO by Griess assay and (c) TNF-α by ELISA. Data are presented as the mean ± SEM (n = 4–7). *$p < 0.05$ compared with the control group, $^{\#}p < 0.05$ compared with the value following TMT treatment alone. C: control, M: magnolol, T: TMT, T+M: TMT + magnolol

(a)

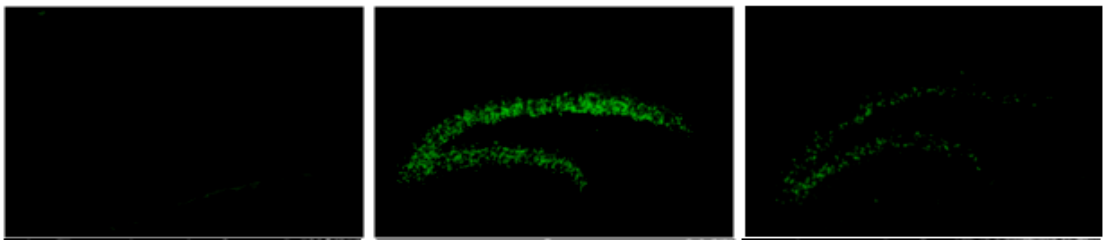

(b) (c) (d)

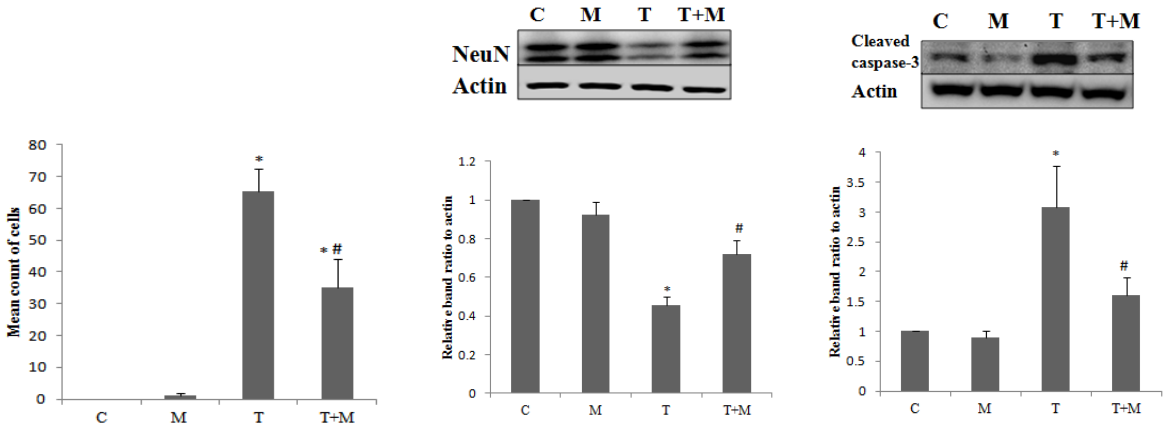

Fig. 9. Magnolol protected against TMT-induced hippocampal neuronal cell death. (a) Hippocampal slices obtained from mice two days after TMT treatment were stained with Fluoro-Jade B (FJB). Each stained tissue section was imaged using a fluorescence microscope and a 100x objective. (b) Fluorescence intensity was quantified using Image J software. Tissues obtained at day 2 were subjected to Western blot analysis for (c) NeuN, and (d) cleaved caspase-3. The bar graphs in the Western blot analysis represent the band intensities of NeuN and cleaved-caspase 3 normalized to actin. Data are presented as the mean ± SEM (n = 5–7). *$p < 0.05$ compared with the control group, $^{\#}p < 0.05$ compared with the value following TMT treatment alone. C: control, M: magnolol, T: TMT, T+M: TMT + magnolol

(a) (b)

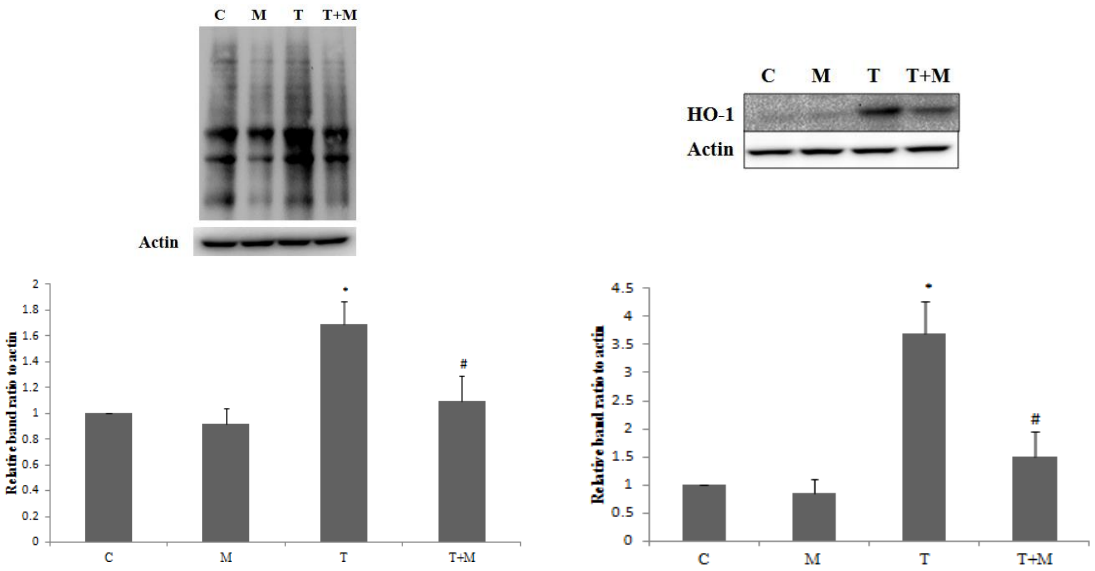

Fig. 10. Magnolol suppressed TMT-induced oxidative stress in the hippocampus. Tissues obtained from mice 2 days after TMT treatment were subjected to Western blot analysis of (a) protein carbonylation, and (b) HO-1 expression. The bar graphs represent the band intensity of protein carbonyls and HO-1 normalized to actin. Data are presented as the mean ± SEM (n = 7). *$p < 0.05$ compared with the control group, $^{\#}p < 0.05$ compared with the value following TMT treatment alone. C: control, M: magnolol, T: TMT, T+M: TMT + magnolol

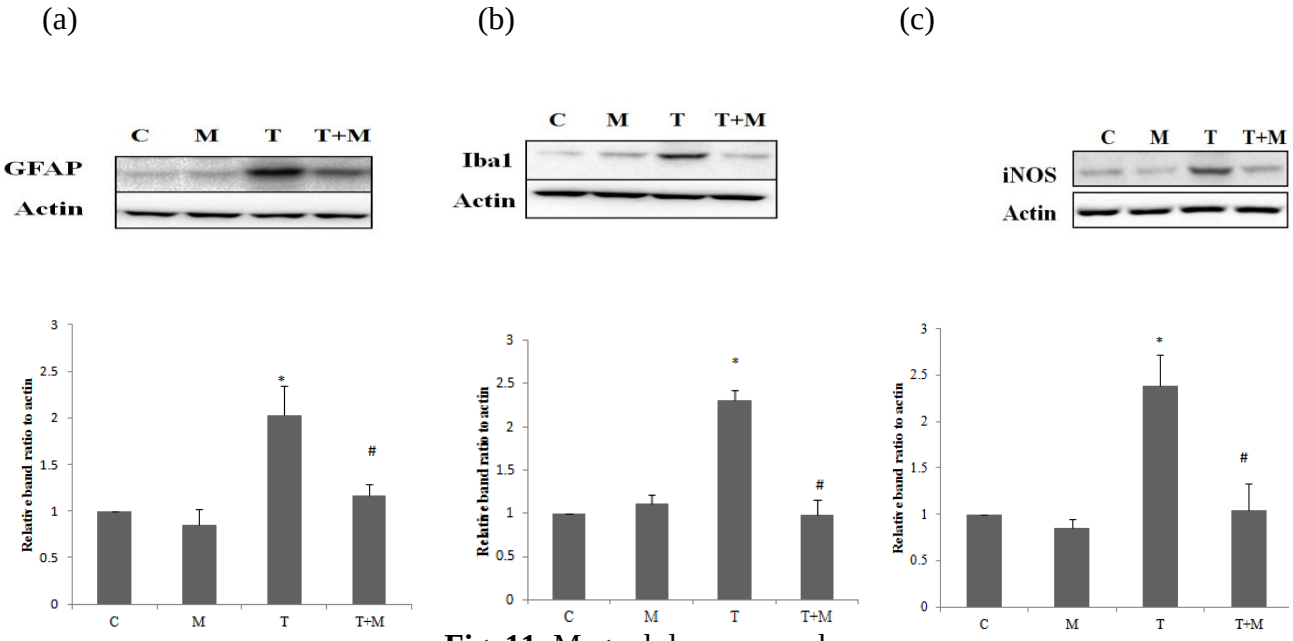

Fig. 11. Magnolol suppressed TMT-induced glial activation and iNOS in the mouse hippocampus. Tissue obtained from mice 2 days after TMT treatment were subjected to Western blot analysis. The bar graph represents the band intensity of (a) GFAP, (b) Iba1, and (c) iNOS normalized to actin. Data are presented as the mean ± SEM (n = 5). *$p < 0.05$ compared with the control group, $^{\#}p < 0.05$ compared with the value following TMT treatment alone. C: control, M: magnolol, T: TMT, T+M: TMT + magnolol

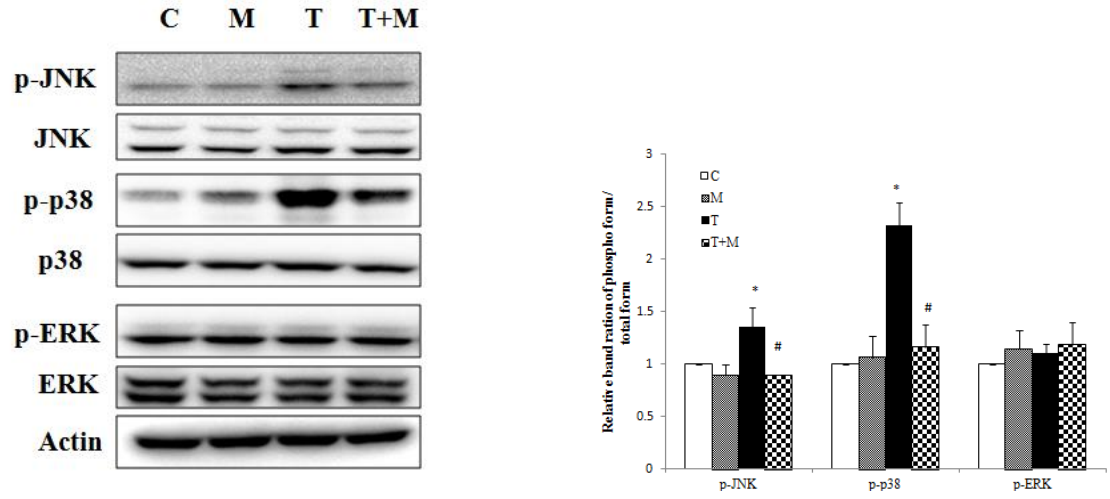

Fig. 12. Magnolol suppressed TMT-induced p-JNK and p-p38 expression in the mouse hippocampus. Tissue obtained from mice one day after TMT treatment was subjected to Western blot analysis. The bar graph represents the band intensity of p-JNK, p-ERK, and p-p38 normalized to total. Data are presented as the mean ± SEM (n = 7). *$p < 0.05$ compared with the control group, $^{\#}p < 0.05$ compared with the value following TMT treatment alone. C: control, M: magnolol, T: TMT, T+M: TMT + magnolol

Graphs

Fig. 1 (a)

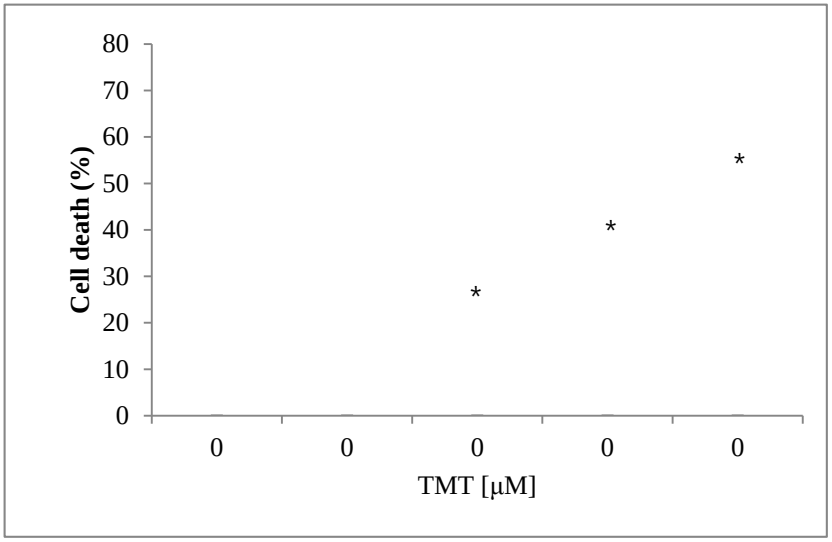

Fig. 1
(b)

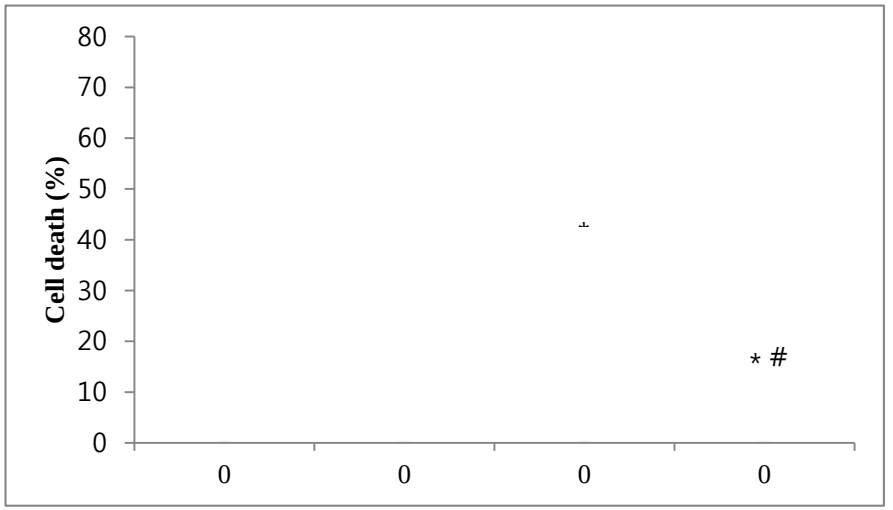

Fig. 2
(a)

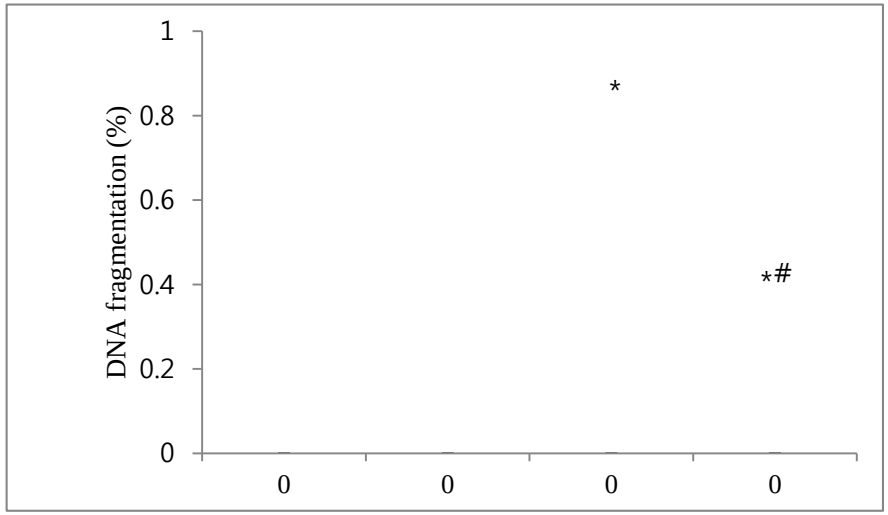

Fig. 2
(b)

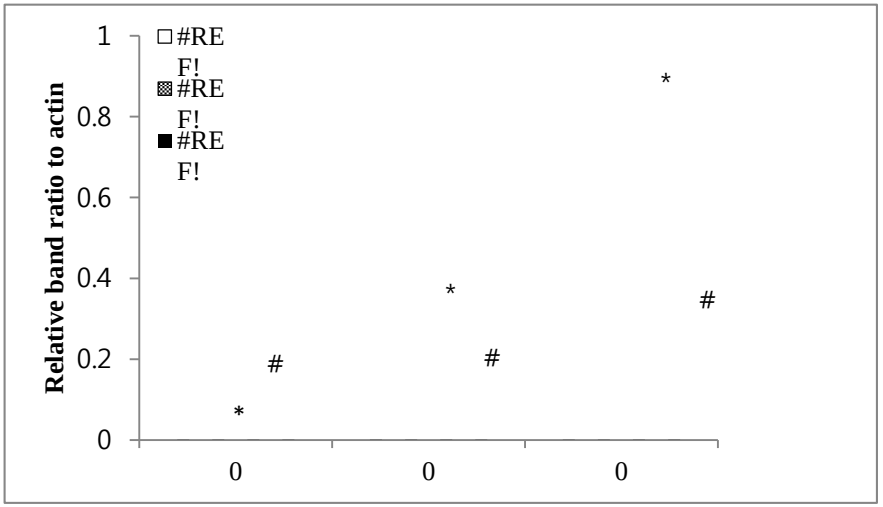

Fig. 3 (a)

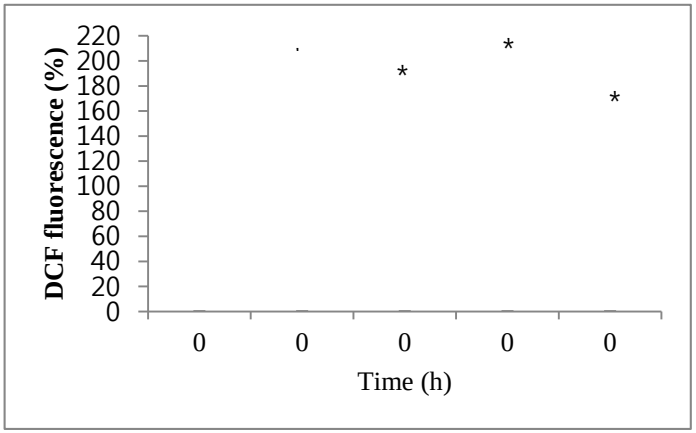

Fig. 3 (b)

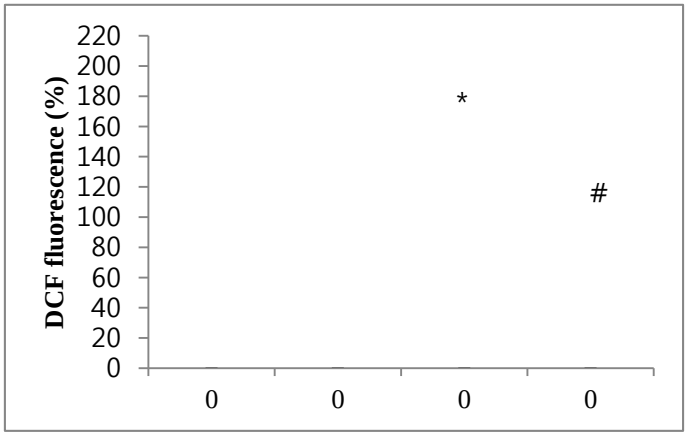

Fig. 4 (a)

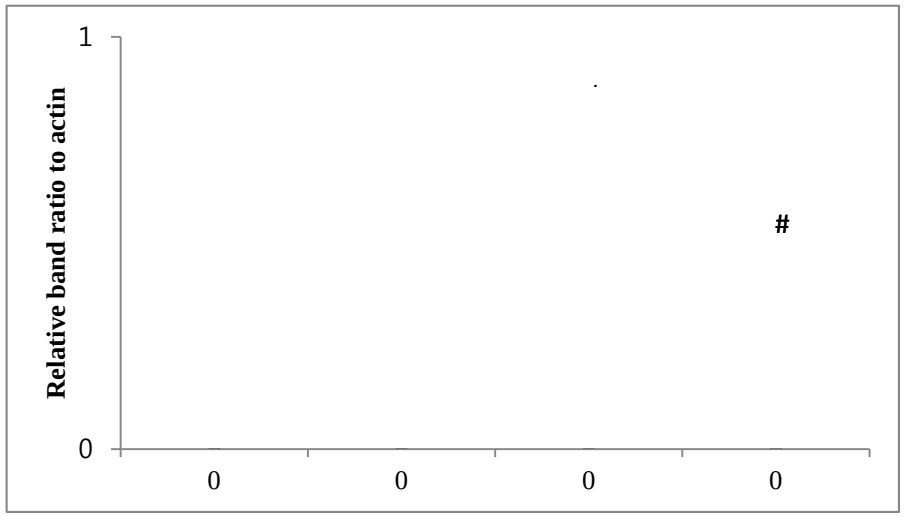

Fig. 4
(b)

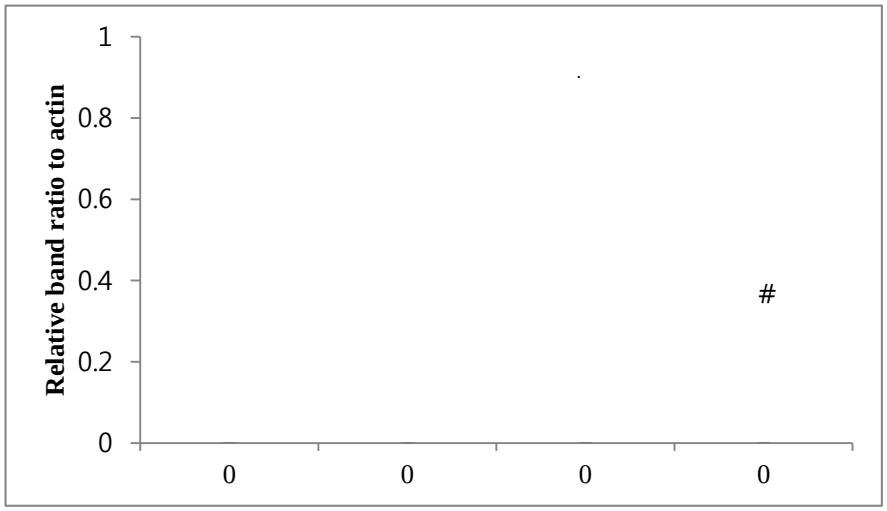

Fig. 5 (a)

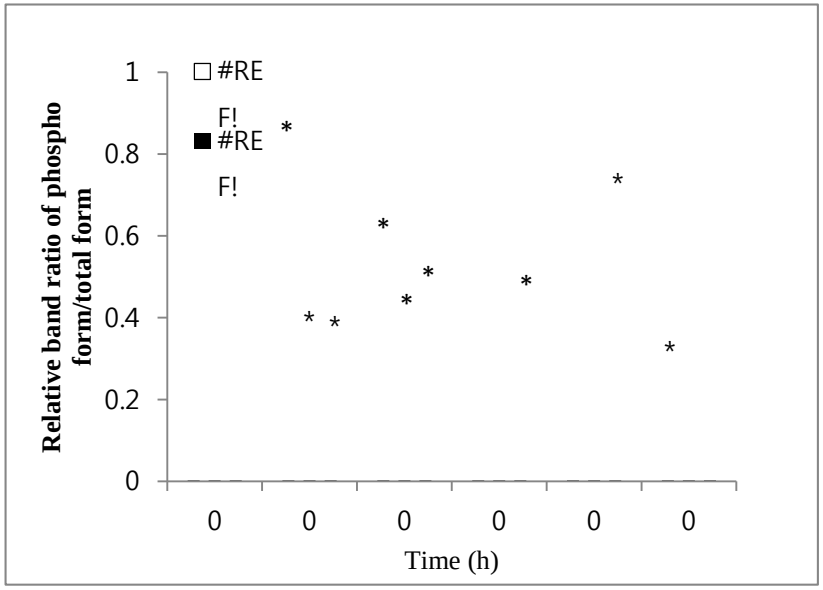

Fig. 5 (b)

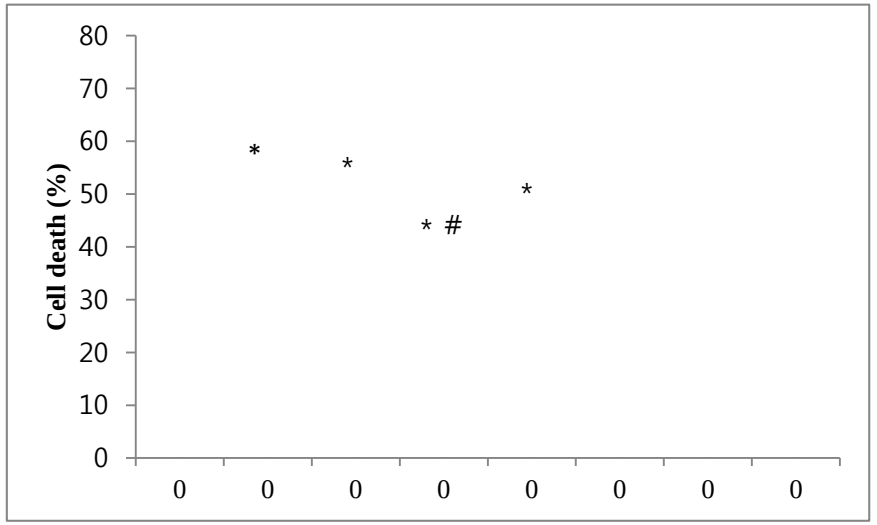

Fig. 6

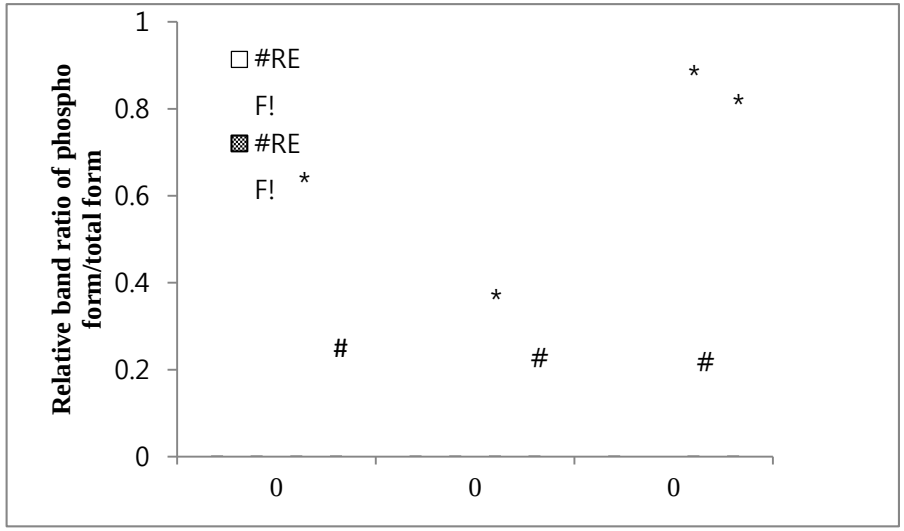

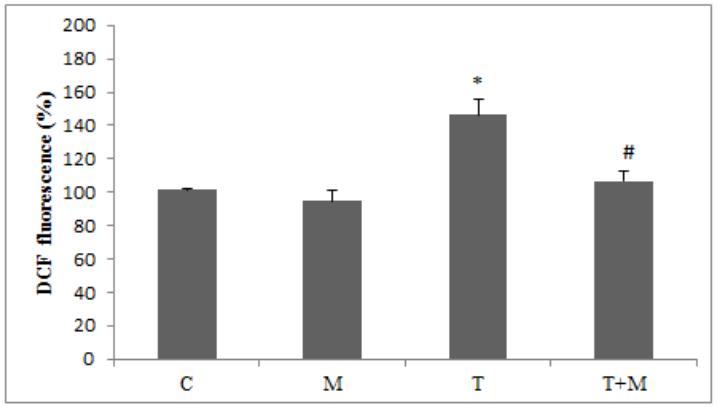

Fig 7a

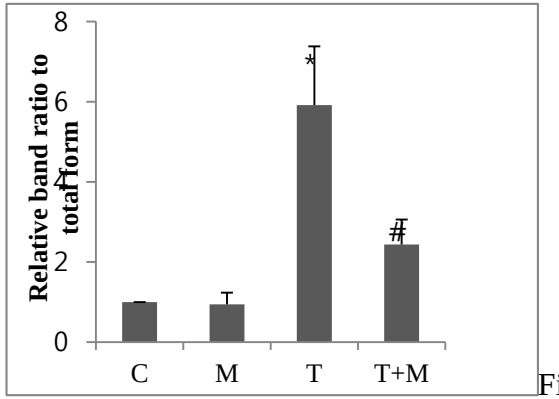

Fig 7b

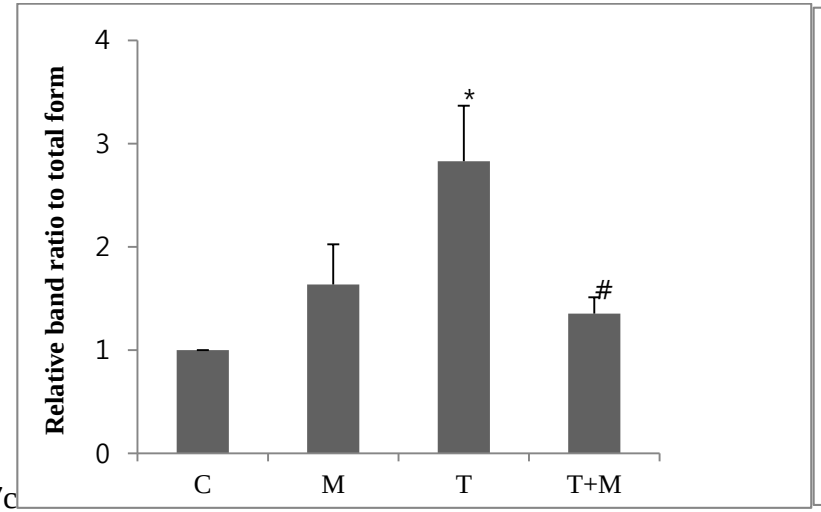

7c

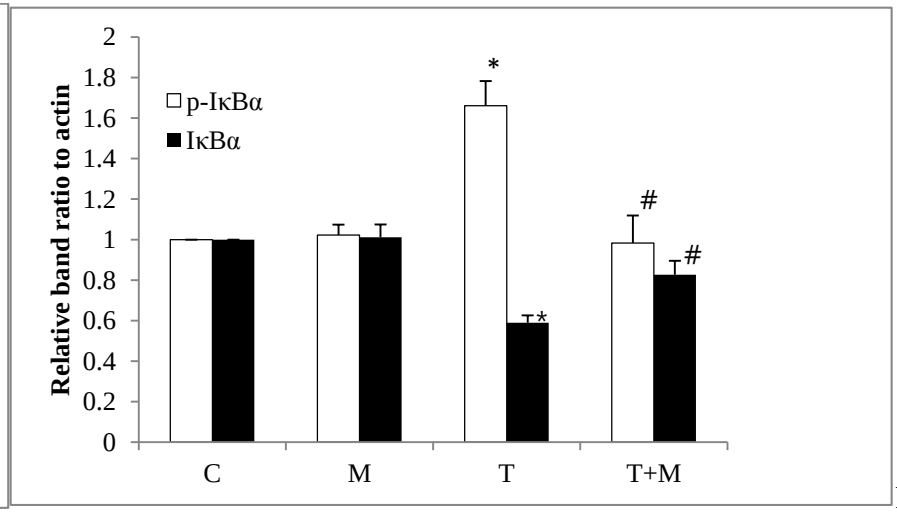

Fig 7d

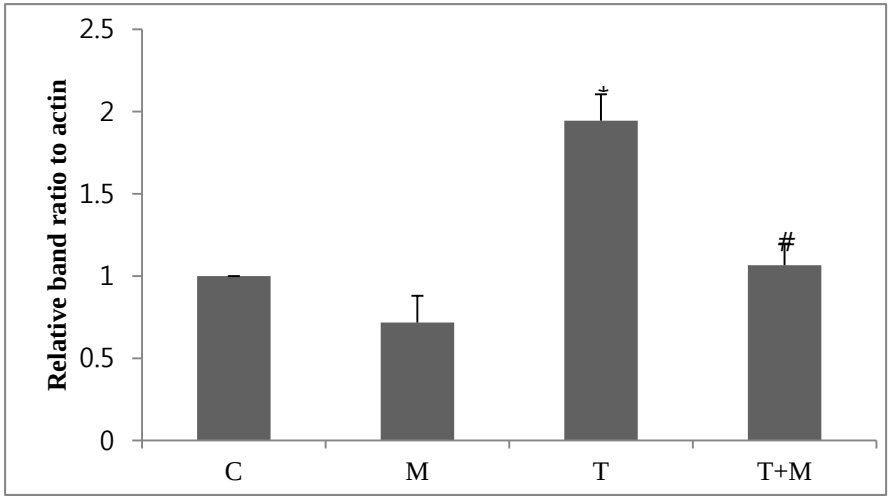

Fig8a

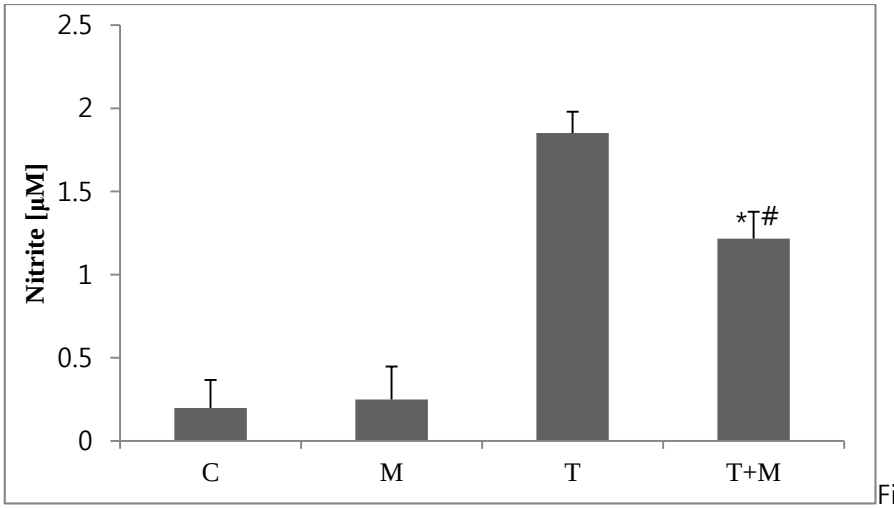

Fig 8b

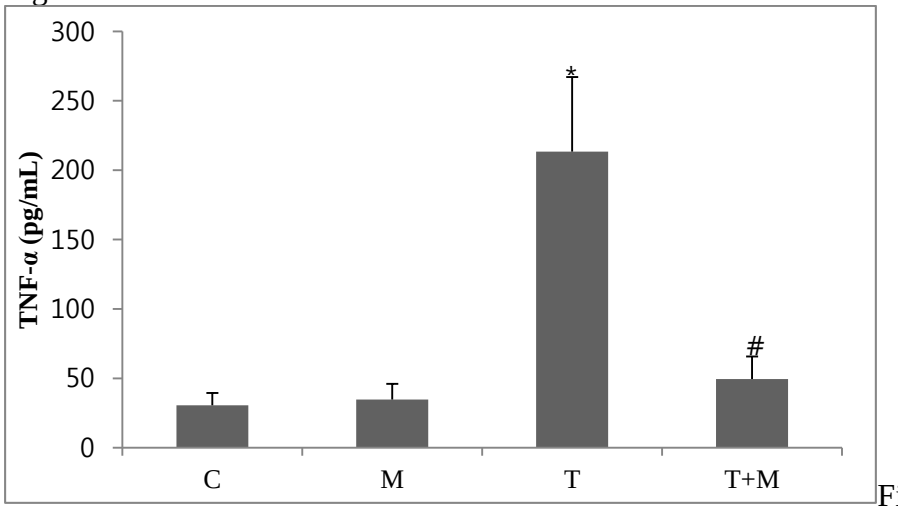

Fig 8c

Fig. 9
(b)

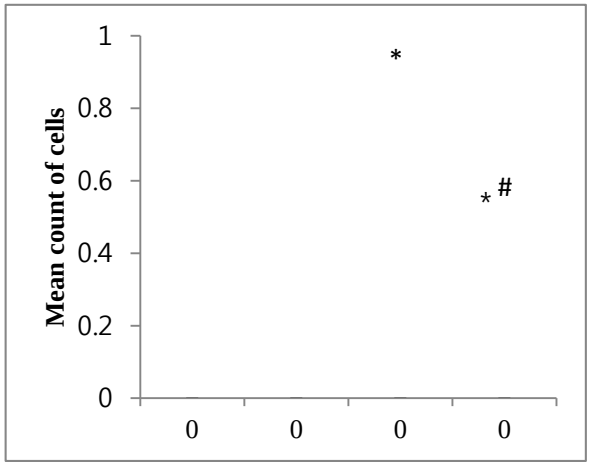

Fig. 9 (c)

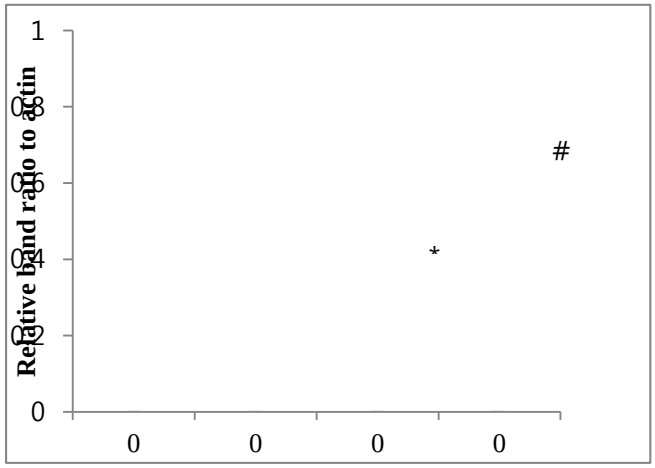

Fig. 9
(d)

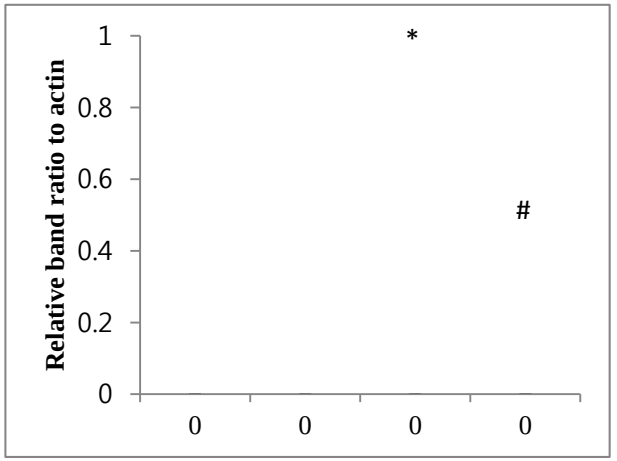

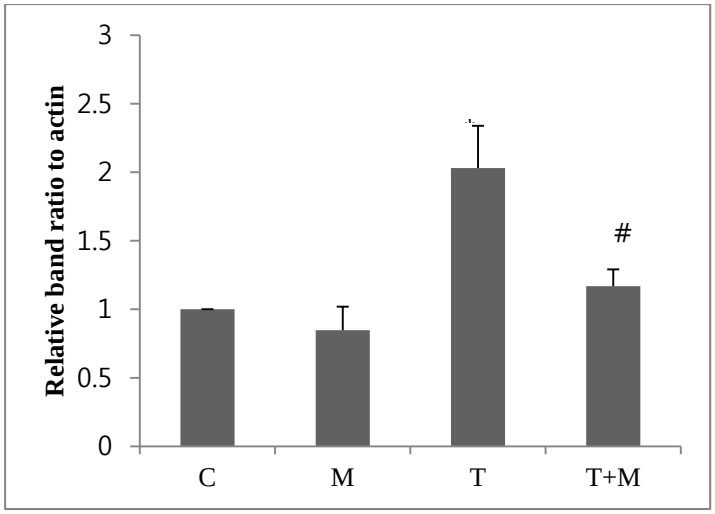

Fig 11 a

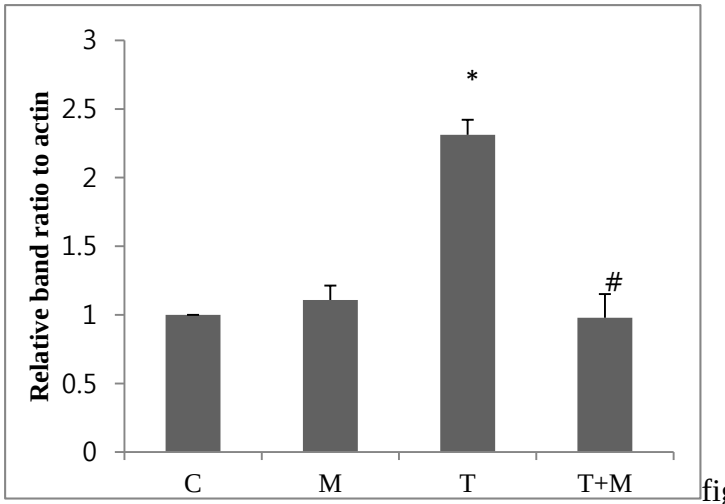

fig 11 b

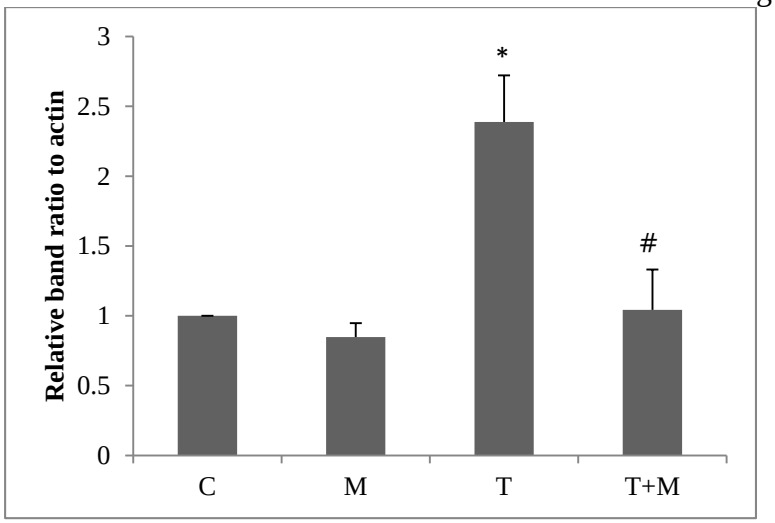

Fig 11c

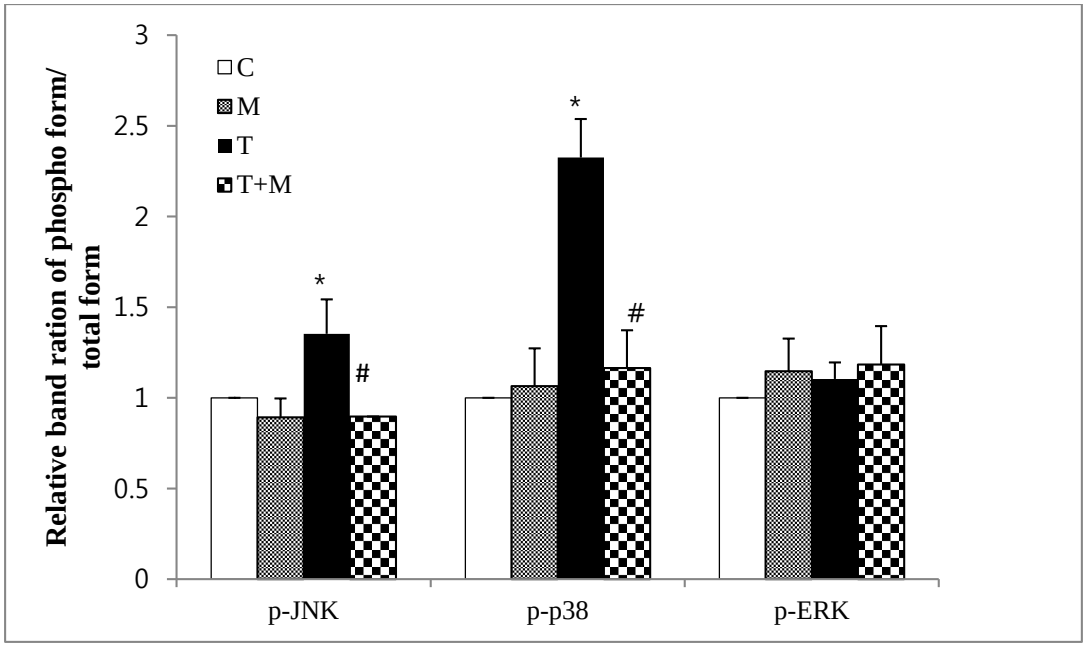

Fig 12